Lawrence Berkeley National Laboratory
LBL Publications

Title
Bridging Nanoscopic Surface Heterogeneity and Macroscopic Nucleation Rates: A Perspective on Probabilistic Approaches

Permalink
https://escholarship.org/uc/item/3369n6zv

Journal
Crystal Growth & Design, 26(18)

ISSN
1528-7483

Authors
Hellevang, Helge
Fischer, Cornelius
Nooraiepour, Mohammad
et al.

Publication Date
2026-09-16

DOI
10.1021/acs.cgd.6c00312

Copyright Information
This work is made available under the terms of a Creative Commons Attribution License, available at https://creativecommons.org/licenses/by/4.0/

Peer reviewed

eScholarship.org Powered by the California Digital Library
University of California

CRYSTAL GROWTH & DESIGN

pubs.acs.org/crystal

Perspective

Open Access

This article is licensed under CC-BY 4.0

Bridging Nanoscopic Surface Heterogeneity and Macroscopic Nucleation Rates: A Perspective on Probabilistic Approaches

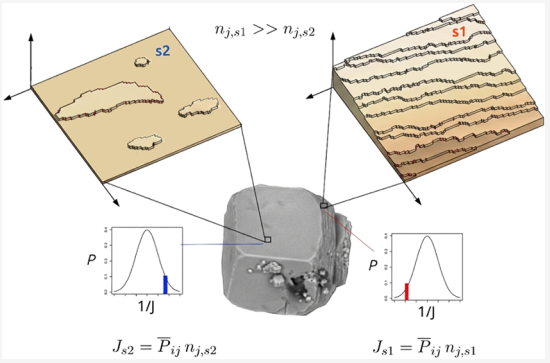
Helge Hellevang,* Cornelius Fischer, Mohammad Nooraiepour, Sergi Molins, Mohammad Masoudi, and Nikolaos I. Prasianakis

Cite This: *Cryst. Growth Des.* 2026, 26, 7321−7336

Read Online

ACCESS | Metrics & More | Article Recommendations

ABSTRACT: Predicting the number of newly formed crystals and their spatial distribution on surfaces or within pore spaces matters across many fields, from structural biology to coupled fluid flow and reactive transport in porous media to atmospheric physics. Nucleation occurs at molecular and nanoscopic scales, yet classical nucleation theory (CNT) provides an averaged, macroscopic description, and a growing body of experimental observations is inconsistent with CNT predictions. Probabilistic nucleation models have been developed to predict mineral formation in reactive porous geochemical systems and to generate uncertainty estimates, for example, of how mineral growth affects fluid flow. However, the probability density functions of nucleation rates or induction times that underlie these models remain poorly constrained and are not grounded in the intrinsic nanoscopic physicochemical mechanisms underlying the observed macroscopic behavior. This perspective reviews recent advances in mineral nucleation research, focusing on modeling in coupled reactive transport systems, and examines how the large uncertainties reported for macroscopic nucleation rates may be linked to the extent and spatial distribution of surface sites with contrasting reactivity, such as kinks, steps, and terraces. Building on this, we propose a framework that integrates site-specific nucleation probabilities and explicitly accounts for polymorph selection to enable deterministic prediction of macroscopic nucleation rates from intrinsic surface properties. While the resulting parameter space is extensive, recent advances in machine learning, combined with high-throughput experimentation and simulation, suggest that such predictive, multiscale models are now within reach.



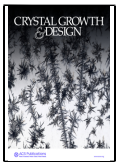
1. INTRODUCTION

Newly formed minerals and amorphous materials, microscopic in size yet macroscopic in consequence, shape critical processes across engineering, Earth and environmental science, and medicine. Nucleation governs the hydration of cement and geopolymers,[1−3] the degradation of automotive batteries,[4−6] the processing of rare earth elements from brines,[7−9] the fouling of desalination membranes,[10,11] mineral scaling in geoenergy resources and geothermal wells,[12,13] and the formation of fluid flow barriers during geological CO_2 storage (GCS) or hydrothermal operations.[14−19] Across these settings, it is typically the invasion of reactive fluids into porous media that drives nucleation, and the resulting medium evolution in turn alters how fluid flows, with consequences such as a drop in well injectivity. This deeply coupled nature of fluid flow, solute transport, and mineral formation underlies the pressing need to predict where and when crystals appear.

Despite this importance, predicting nucleation rates remains challenging. Predicting nucleation events that occur at the nanometer scale yet affect macroscale behavior is inherently difficult, and classical nucleation theory (CNT), the macroscale model commonly used to compute nucleation rates, has several limitations. Its predictions are increasingly inconsistent with experimental observations, particularly at low supersaturations or on heterogeneous substrates.[20−25] Nonclassical models, including multistep preclustering, dense liquid precursors, and spinodal decomposition, can overcome some of these macroscale limitations,[20,22−24,26−32] but a comprehensive model that effectively bridges scales is still lacking. Such a model is needed if nucleation is to be treated not as an isolated process but as a process coupled to geochemical reactive transport in natural and engineered media.

The prominent example of calcium carbonate (CC), a key component of the global carbon cycle, a target mineral for geological CO_2 storage,[33] and a widely used model system for

Received: March 5, 2026
Revised: July 23, 2026
Accepted: July 27, 2026
Published: August 6, 2026



ACS Publications

© 2026 The Authors. Published by American Chemical Society

https://doi.org/10.1021/acs.cgd.6c00312
Cryst. Growth Des. 2026, 26, 7321−7336

Downloaded from pubs.acs.org/cgdefu/article-pdf/26/18/7321/6451959/acs.cgd.6c00312.pdf by guest on 19 October 2026

crystal growth,[34,35] illustrates these issues well. While CC nucleation has received much attention and much is known, discussion of specific nucleation mechanisms and classical versus nonclassical pathways remains very active in the literature.[20,23,24,26,27,32,36−40] The CC phase that grows, whether amorphous CC (ACC), or crystalline vaterite, calcite, or aragonite, is primarily thermodynamically controlled,[20,32,38,39] but in some cases, especially at elevated supersaturations, several CC polymorphs may form simultaneously.[36,40−42] Figure 6 illustrates this directly: reflected light microscopy of CC nucleated on a polished glass plate at high supersaturation shows spherical, rhombohedral, and needlelike crystals, consistent with vaterite, calcite, and aragonite forming concurrently from the same solution under nominally identical surface conditions. Polymorph selection and distribution may alternatively be controlled by growth once a critical nucleus size is exceeded, as has been suggested for nucleation from Lennard-Jones fluids.[43]

These observations raise a fundamental question: can such multipolymorph, multipathway phenomena be predicted? More specifically, what factors control the nucleation pathway and the transitions between classical and nonclassical behavior, and what role does the substrate surface play in these choices? Despite the wealth of CC nucleation and growth experiments and a good understanding of nucleation pathways even at the molecular scale, we still lack a complete picture of what controls heterogeneous nucleation.

We argue that a fundamental source of this difficulty has been largely overlooked: the surface itself. Even surfaces that appear macroscopically uniform, such as a polished glass plate or a cleaved mineral face, are nanoscopically heterogeneous. Kink sites, step edges, terraces, dislocations, and etch pits each present a distinct local geometry, electronic structure, and coordination environment, and each offers a different energy barrier for nucleation.[44−47] The large uncertainties commonly reported for macroscopic nucleation rates may largely reflect this heterogeneous spatial distribution and density of surface sites. Classical nucleation theory subsumes all of this into a single, spatially averaged interfacial free energy, $\hat{\sigma}_{ij}$, discarding the very information that determines where nucleation actually occurs and why measured rates vary by orders of magnitude across nominally identical experimental conditions. We propose that this nanoscale surface heterogeneity is not a nuisance to be averaged away, but the physical origin of macroscopic nucleation variability, and therefore the key to predicting it.

In this context, this perspective pursues a 2-fold objective, developed in four steps. First, it surveys recent research on how nanoscale variations in surface structure and chemistry control nucleation behavior. Rather than treating a mineral surface as uniform, explicitly accounting for nanoscale heterogeneity helps explain localized "hot spots" and the significant deviations between experimental rates and classical macroscopic models. Second, it explores the feasibility of deterministically predicting macroscopic nucleation rates from these intrinsic, nanoscale surface properties. We begin by reviewing classical and nonclassical nucleation frameworks, focusing on the role of the substrate and on the limitations that motivate a more surface-aware approach (Section 2). We then examine how intrinsic variability in surface reactivity, quantifiable through dissolution-rate spectra, AFM, and vertical scanning interferometry, persists as a steady-state property of real mineral surfaces and sets a baseline for nucleation-site heterogeneity (Section 4.1). Building on this foundation, we introduce a multisite, multipolymorph nucleation model (Section 4.2) that replaces the averaged interfacial free energy with an explicit sum over site types and polymorphs, each weighted by its nucleation probability and surface density, providing a physically grounded basis for constraining the probability density functions used in existing macroscopic models and for understanding their inherent uncertainty. Finally, we discuss perspectives on implementation and parametrization of the proposed model, including the role of machine learning, automated experimentation, and reactive transport modeling (RTM) in making this approach tractable for realistic systems (Section 5). Together, these sections trace a path from nanoscopic surface physics to macroscopic nucleation rates, a path that, with recent advances in computation and data acquisition, is now within reach.

2. CLASSICAL VERSUS NONCLASSICAL HETEROGENEOUS NUCLEATION

The nucleation rate of minerals in aqueous solutions can be described by

$$J_s = k_N \exp\left(-\frac{\Gamma \hat{\sigma}_{ij}^3}{T^3(\ln\ \Omega)^2}\right) \quad (1)$$

where J_s is the nucleation rate (no. nuclei/s), k_N is the pre-exponential factor or rate constant, Γ is a parameter combining the molar volume of the nucleating phase, Boltzmann's constant, and a geometry factor (e.g., spherical), $\hat{\sigma}_{ij}$ is the effective interfacial free energy, T is absolute temperature, and Ω is the saturation ratio of the solution with respect to the nucleating phase.

The effective interfacial free energy is different from the theoretical interfacial free energy derived from the direct attachment mechanism in the classical nucleation theory, which is violated for a number of CC phases forming in a nonclassical way by preclustering[22,23,26,27] or through metastable dense liquid phases.[28−30] However, the formation of prenucleation clusters (PNCs) remains debated, as transition-state configurations do not appear to be consistent with PNCs.[24] The pre-exponential factor k_N can also be expanded to account for factors that affect the interaction frequency at the nucleation stage. With these considerations, eq 1 could in principle apply to any nucleation pathway.

The least understood factor in heterogeneous nucleation, whether it proceeds via a classical or nonclassical pathway, is the substrate surface. On the macroscopic scale, the surface appears homogeneous, and the spatial distribution of secondary precipitates seems random.[48,49] This is not the case. The surface will always have various defects at the nano- and microscale that confer a different nucleation probability than on an atomistically flat surface. These reactive sites and their roles are not explicitly captured in eq 1, as the interfacial free energy of the surface is an averaged property. (Section 4.1 addresses in detail the role of such surface sites.)

This bears a conceptual similarity to the well-established multisite sorption models, where surface heterogeneity, such as frayed edge sites (Sawhney, 1972), planar sites, and interlayer sites, is explicitly accounted for as distinct parameters. Different types of sorption sites are characterized by distinct coordination numbers and binding energies for ions and complexes. Similarly, it is to be expected that, at the atomic level, local interfacial energies, contact angles, surface rough-

Downloaded from pubs.acs.org/cgdefu/article-pdf/26/18/7321/6451959/acs.cgd.6c00312.pdf by guest on 19 October 2026

https://doi.org/10.1021/acs.cgd.6c00312
Cryst. Growth Des. 2026, 26, 7321−7336

ness, and lattice characteristics will provide varying degrees of reduction in the nucleation barrier, playing a significant role in the rate of nucleation.

Asymmetric ionic solutions, i.e., solutions that are far from the stoichiometric [cation]/[anion] ratio of the salt, strongly affect rates of crystal growth,[50−55] as well as the nucleation itself.[54−56] Asymmetric ionic solutions should favor the formation of both nonstoichiometric PNCs and amorphous phases such as ACC over crystalline phases, but the extent of this is not known. We consider the potential influence of the substrate surface and the near-surface chemical environment on the formation of nonstoichiometric nuclei particularly intriguing, as this remains poorly understood.

Nonclassical pathways are formally integrated into nucleation theory through two principal approaches. The first retains the mathematical structure of eq 1 but shifts the thermodynamic framework to a metastable precursor phase (e.g., an amorphous or dense liquid phase) rather than the final crystalline polymorph.[28,30,57−59] In this formalism, $\hat{\sigma}_{ij}$ represents the interfacial free energy of the fluid-precursor interface rather than that of the final polymorph, because this value is typically lower than the fluid-crystal interfacial free energy, the thermodynamic nucleation barrier (ΔG^*) is significantly reduced, making initial phase separation favorable even at a saturation ratio Ω for which direct nucleation of the crystalline phase would be highly unfavorable. The subsequent transformation of the precursor into the stable crystal is then treated as a separate, solid-state or solution-mediated phase transition.

The second approach uses explicit two-step nucleation formalisms,[60,61] in which the free energy landscape features a local intermediate minimum corresponding to a dense liquid or prenucleation cluster (PNC) state.[26,27,62] Here, the overall nucleation rate is no longer governed by a single exponential term as in eq 1, but is instead a coupled kinetic function of both the rate of precursor formation and the rate of the subsequent internal structural rearrangement or desolvation required to nucleate the crystalline phase from within the precursor. Depending on solution conditions, either the initial phase separation or the secondary restructuring step acts as the rate-limiting kinetic bottleneck.

3. PROBABILISTIC NUCLEATION MODELS IN REACTIVE TRANSPORT

3.1. Historical Development of Probabilistic Models

The stochastic nature of nucleation has been recognized since the theoretical foundation of classical nucleation theory was laid by Volmer, Frenkel, and Becker between 1929 and 1945.[63−66] A short summary of the developments in probabilistic models for heterogeneous nucleation, building on these pioneering works, is provided in Table 1.

In 1952, Pound and La Mer[67] demonstrated that the probability of nucleation at microscopic impurities from a macroscopic perspective followed a Poisson distribution. Twenty years later, Toschev et al.[68] developed an analytical model for nucleation and demonstrated that the randomness of induction time seen for heterogeneous nucleation can be used to predict transient and stationary rates of nucleation. In 2008, Curcio et al.[69] demonstrated that different polymorph phases will have different probabilities of forming due to slight differences in the Zeldovich factor (in CNT, the Zeldovich factor Z represents the probability of a nucleus at critical size to continue growth or redissolve). In 2020, Fazeli et al.[48]

Table 1. Review of Probabilistic Nucleation Models and Historical Developments

Year	Authors/Approach	Contributions
1929−1945	Volmer, Frenkel, Becker, Zeldovich.[63−66,71] Fundamentals of nucleation	Theoretical developments for the later probabilistic models; stepwise addition of single molecules (=CNT) occur by statistical energy fluctuations.
1952	Pound and La Mer.[67] Nucleation from supercooled droplets of tin. Microfluidics.	Nucleation rates, controlled by the number of impurity particles in the droplets, follow a Poisson distribution; equal probability to nucleate at each of these centers (sites); nucleation rates decrease over time as the number of available sites is reduced.
1972	Toschev et al.[68] Probabilistic aspects of the nucleation process	Randomness of induction times; use of distribution of induction times to quantify nucleation given experimental data; semianalytical procedure to calculate stationary nucleation rates and induction times, building on CNT.
2008	Curcio et al.[69] Probabilistic aspects of polymorph selection by heterogeneous nucleation on microporous hydrophobic membrane surfaces	Different probabilities of heterogeneous nucleation of two paracetamol polymorphs are different; difference is related to the Zeldovich factor; theoretical expression of the Zeldovich factor.
2020	Fazeli et al.[48] Gaussian Induction Time (GIT) model. Pore-scale model of mineral nucleation−growth	First implementation of a probabilistic nucleation model in a reactive transport model; probability of a nucleation event for each surface site follows a Gaussian distribution of induction times, based on the CNT.
2021	Starchenko.[70] Pore-scale modeling of mineral nucleation−growth	Simulations of nucleation and growth; effect of Pe- and Da-numbers on the nucleation−growth patterns; nucleation probability for each surface site a function of time and nucleation rate, based on the CNT)
2026	Hellevang et al. (this work). A multisite polymorph-selective nucleation model	Hypothesis: Macroscopic variability in heterogeneous nucleation rates arises primarily from differences in the density and spatial distribution of favorable surface nucleation sites on the substrate. Introduces a model in which the probability of successful nucleation differs across surface sites (steps, kinks, pits, etc.). Both nonclassical and classical nucleation pathways are considered.

Downloaded from pubs.acs.org/cgdefu/article-pdf/26/18/7321/6645959/acs.cgd.6c00312.pdf by guest on 19 October 2026

https://doi.org/10.1021/acs.cgd.6c00312
Cryst. Growth Des. 2026, 26, 7321−7336

published the first implementation of a probabilistic mineral nucleation model in a reactive transport model, and two years later, Starchenko[70] followed up with an alternative probabilistic nucleation model. The latter two models, which connect probabilistic crystal nucleation to reactive transport and serve as the starting point for several subsequent models, are described in more detail below.

The probabilistic nucleation model suggested by Fazeli et al.[48,49] (hereafter referred to as the Gaussian Induction Time (GIT) model) proposes that at the macroscopic scale, the precise spatial distribution of nuclei cannot be deterministically predicted. Instead, for any given small surface area (or "spot"), the induction time required for the formation of the first nucleus is treated as a random variable following a Gaussian distribution centered on the mean (deterministic) induction time. Consequently, over sufficiently large surfaces and extended time scales, the cumulative number of nuclei is symmetrically bounded between 0 and twice the mean induction time, reflecting the probabilistic symmetry of the Gaussian distribution:

$$P(x) = \frac{1}{\sigma\sqrt{2\pi}}\exp\left(-\frac{(x-\tau_N)^2}{2\sigma^2}\right);\ 0 < x < 2\tau_N \quad (2)$$

where τ_N is the mean induction time (time/nucleus), and σ is the standard deviation of the random variable x ($\sigma = \tau_N/4$). To find the probabilistic induction time (τ_p) for each surface spot (area), a random number p ($0 < p < 1$) is generated and τ_p is found from the cumulative density function F from $\tau_p = F^{-1}(p)$. In the GIT model, the underlying probability density function is assumed to be Gaussian, symmetric around the mean (deterministic) induction time τ_m. This shape is chosen on the grounds that nucleation is treated as a fully stochastic natural process with no strong directional bias in the variability of induction times.

The model proposed by Starchenko[70] also expresses the probability of forming a nucleus on a specific area as a function of the nucleation rate based on the CNT:

$$P(J,\ t) = 1 - \exp(-J\Delta t) \quad (3)$$

where $J = J_s S$, S is surface area, and J_s is the nucleation rate (eq 1). This model reproduces the increasing probability of nucleation in a specific area over time, as well as the mean long-term number of crystals when $J\Delta t \ll 1$. This implies that the model performs well for both small (pore-scale) and large (continuum-scale) systems when using small time increments (Figure 1). Pore-scale models resolve the actual geometry of pores and grains, while continuum-scale models treat the porous medium as a "smoothed" material with averaged properties (e.g., porosity, permeability, mass of secondary crystals). One fundamental difference between the Starchenko and the GIT models is that the former will have the same probability for all surface sites in a pore-scale model (given a homogeneous T, Ω, k_N, and $\hat{\sigma}$), while the latter will have a Gaussian distributed probability for each discrete surface area, also for homogeneous surfaces with uniform $\hat{\sigma}$. Another difference is that the Starchenko model can only work for pore-scale models where $J\Delta t \ll 1$ (Figure 1), while the GIT model in principle can be used at both pore-scale and continuum-scale, as the input variable in the Gaussian distribution is the probabilistic induction time, and the total number of nuclei during a time step can be found from $S\Delta t/\tau_p$, where S is surface area. In the Starchenko model, the exponent ($J\Delta t$) is not unitless. While this does not affect the flexibility of the model to predict the number and spatial distribution of nuclei, it must be noted that $P = 0.63$ at $J\Delta t = 1$, which may lead to under-prediction of long-term nucleation rates. For large systems and for systems with rapid nucleation, and when large time steps are considered, the model must be used with caution. The drawback of both models is that their probability density functions are insufficiently constrained and not grounded in the intrinsic nanoscopic physicochemical constraints that underlie the macroscopic observations.

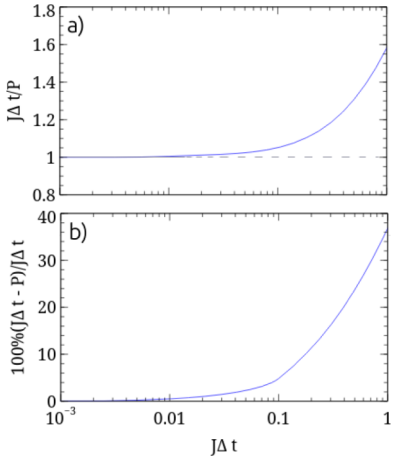


Figure 1. Comparison between long-term (large-size) predicted number of nuclei ($J\Delta t$), and the modeled (=P) using the Starchenko probability (eq 3). a) $J\Delta t$ vs $(J\Delta t)/P$. Values higher than 1 indicate an erroneously predicted number of nuclei. b) Error percentage $(100\%(J\Delta t - P)/J\Delta t)$.

3.2. Implementation in Reactive Transport Models

Reactive transport modeling describes the coupled evolution of fluid flow, solute advection−diffusion, and geochemical reactions within porous or fractured media, such as soils, rocks, aquifers, and engineered materials, where the interplay between transport time scales and reaction kinetics governs the spatial and temporal distribution of mineral phases and solute concentrations.[72−74] Crystal nucleation plays a vital role in reactive transport as it controls the initial rate of mineralization,[15,75] and controls changes in porosity, permeability, and flow paths.[76−78]

The first implementation of mineral nucleation in RTMs was by Steefel and Van Cappellen in 1990,[75] combining CNT with crystal growth and Ostwald ripening in a continuum-scale model that also considered 1D advection-diffusion-dispersion of solutes. This pioneering study extended previous research, which treated crystal growth as a local-equilibrium phenomenon[79,80] and neglected the role of nucleation in generating surface area for mineral growth. The model also included the ability to track the grain size distribution of the secondary precipitates. It could track the formation of metastable phases, such as halloysite ($Al_2Si_2O_5(OH)_4$), forming before the thermodynamically most stable phases, such as the polymorph kaolinite, due to the lower interfacial free energy and hence faster nucleation rate of the former. Building on earlier versions, Steefel and colleagues continued to develop RTM capabilities in CrunchFlow/CrunchTope,[81,82] with heterogeneous nucleation appearing in 2017.[83,84] Nearly 30 years after the first implementation, the authors note that "*the lack of thermodynamic and kinetic parameters has certainly limited the*

Downloaded from pubs.acs.org/cgdefu/article-pdf/26/18/7321/6451959/acs.cgd.6c00312.pdf by guest on 19 October 2026

https://doi.org/10.1021/acs.cgd.6c00312
Cryst. Growth Des. 2026, 26, 7321−7336

interest in pursuing this topic in the modeling community." Incorporating nanoscale phenomena, such as heterogeneous nucleation, is, however, essential, even at the continuum scale, to accurately capture the dynamic evolution of macroscopic systems.[83]

Pham et al.[15] proposed a nucleation model for continuum-scale systems, with a single rate expression combining nucleation and growth and combining nucleation parameters into a single effective crystal-substrate pair coefficient. The model highlighted substantial discrepancies in predicted long-term mineralization for CCS systems between the prevailing Transition-State-Theory (TST) frameworks and more realistic models that account for the prolonged induction times of certain minerals at low supersaturations[15,85,88] (Figure 2).

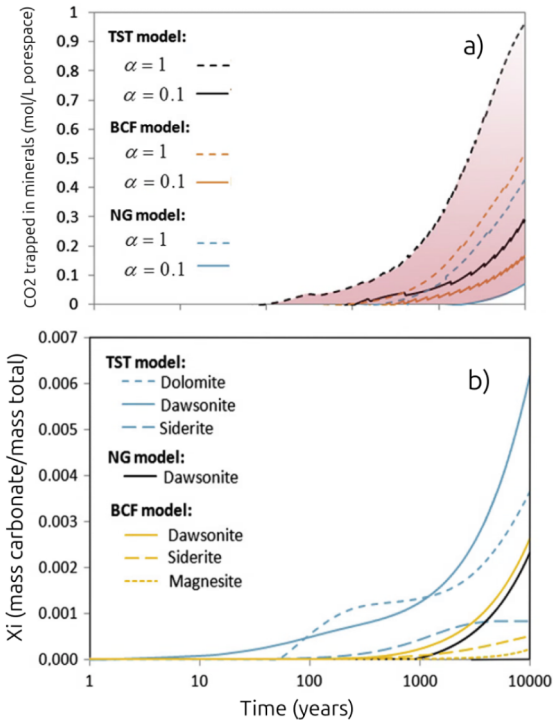


Figure 2. Model comparison of mineralization potential during geological storage of CO_2 (from Hellevang and Aagaard[85]). Three models are compared: a crystal dissolution-growth model based on transition state theory (TST) (see Aagaard and Helgeson,[86] a TST model for dissolution combined with a BCF model[87] for crystal growth, and finally a TST model for dissolution combined with BCF growth and crystal nucleation.[15] Including crystal nucleation results in a more realistic secondary mineralogy, as well as slower and delayed mineral growth, which is also considered more realistic. Modified from Hellevang and Aagaard[85].

Boampong et al.[89] brought the combined nucleation−growth model further forward by fitting nucleation rate parameters (pre-exponential factor, interfacial free energy, and a correction factor) to experimental data on carbon mineralization, and by adding surface passivation for the dissolving phases. The model showed that both nucleation and surface passivation were required to achieve a good match between the model and experimental data. Prasianakis et al.[90] argued that continuum-scale reactive transport simulations cannot reproduce experimental observations without first fitting transport and reaction properties to the experimental data. They introduced a cross-scale concept by implementing CNT in a 2D Lattice-Boltzmann (LB) model to show that adding microscopic (atomic-level) reaction features could reproduce observed macroscopic experimental data well without any empirical prefitting.

The implementations of mineral nucleation and growth up to 2017[83] were all based on deterministic models, i.e., the number of nuclei forming on a surface was always equal to $J\Delta t$. A deterministic spatial distribution of newly formed mineral phases, however, as described above, is only valid for systems reacted at high supersaturations and/or over extended time scales.[49] Experimental works had shown that at low supersaturation, the number of newly formed minerals was few, and it was impossible to predict (numerically) where these minerals formed in the pore-space.[25,91,92] These findings drove the development of probabilistic nucleation models, which were subsequently integrated into both pore- and continuum-scale RTMs.

Fazeli et al.[48] developed a 2D LB model to illustrate the effect of supersaturation and advection rate on the spatial distribution of secondary precipitates. Their model reproduced the expected pattern of patchy precipitates for systems dominated by growth over nucleation ($R_G > R_N$), with uniform dispersed precipitation at high supersaturations and relatively slow growth rates (Figure 3). The uniform coating also seen at low supersaturation in Figure 3a is misleading, as local nucleation and patchy growth patterns will tend to dominate at low supersaturations (e.g., ref 92). In 2021, the 2D LB model was modified and used in Monte Carlo simulations to estimate stochastic variation in crystal nucleation−growth patterns on 2D surfaces and the resulting variation in Shannon entropy.[49]

One core interest in studying systems with mineral dissolution-growth reactions is understanding how the geometry of the solid porous media framework is altered and how the relationship between porosity and permeability changes over time (e.g., refs[78,90,93−95]). A number of empirical and geometric relations have been proposed to track changes in permeability following porosity loss or gain (e.g., refs[96−99]). A 3D LB model based on the GIT model was developed to simulate brine evaporation and the formation of salt aggregates,[77] and to examine the porosity-permeability relationship and the effect of clogging on permeability. The small size of the domain used was a compromise to achieve the desired number of realizations. The simulations showed a large variation in the relation between relative porosity (ϕ/ϕ_0) and relative permeability (k/k_0) for the stochastic simulations, illustrating the uncertainty in porosity-permeability relations derived both from geometric and statistical variations in the spatial distribution of neo-formed phases. The model successfully captured the enhanced probability of secondary nucleation (salt-on-salt precipitation) and the resulting salt aggregation, consistent with laboratory observations.[16]

Deng et al.[100] implemented probabilistic nucleation in their microcontinuum[101,102] pore-scale reactive transport model. While the probabilistic nucleation model was based on the GIT model,[48] their mineral growth model was changed from a deterministic model to one where all new mass grows by heterogeneous nucleation, both nucleation on the foreign substrate (baryte on celestite) and self-nucleation (baryte on baryte nucleation).[100] This process led to the formation of porous aggregates, which reduced the diffusivity of the aqueous solution toward the celestite substrate, thereby influencing both substrate dissolution and the subsequent epitaxial growth

Downloaded from pubs.acs.org/cgdefu/article-pdf/26/18/7321/6645195/acs.cgd.6c00312.pdf by guest on 19 October 2026

https://doi.org/10.1021/acs.cgd.6c00312
Cryst. Growth Des. 2026, 26, 7321−7336

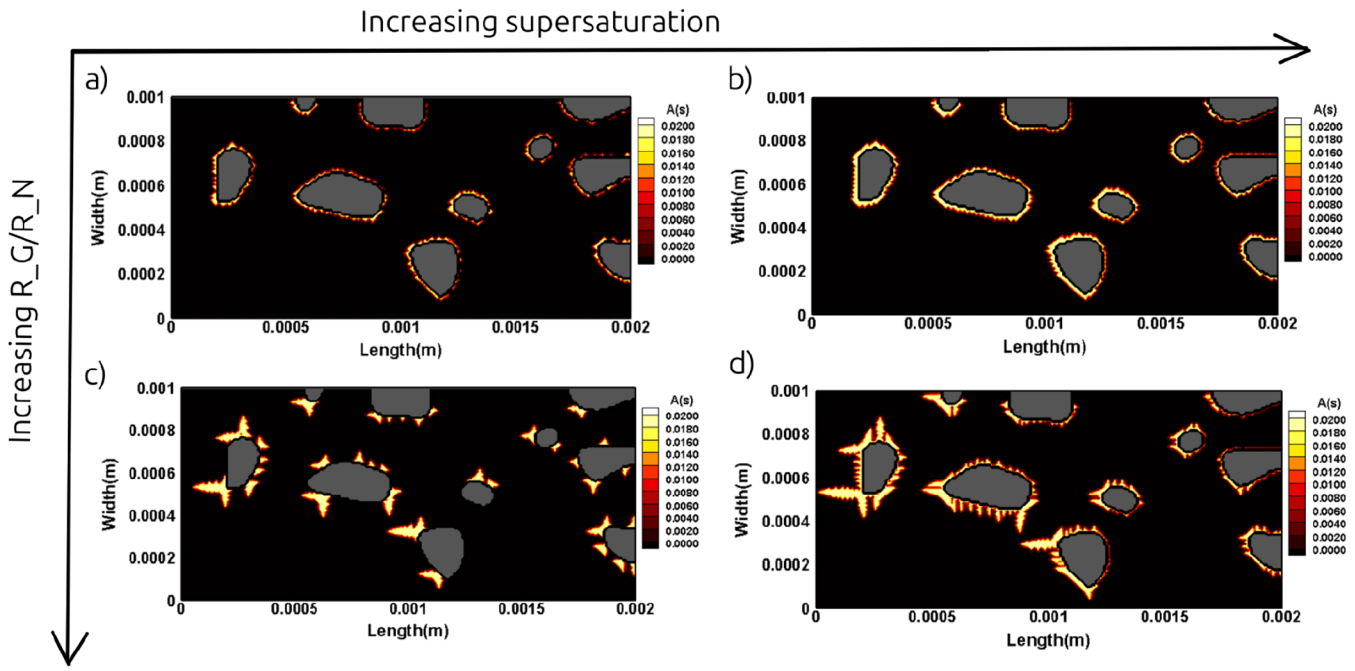


Figure 3. Variation of spatial coverage and growth patterns as a function of supersaturation and relative differences between nucleation and growth rates. Modified from Fazeli et al.[48]

of Barite. While such an approach where nucleation totally dominates the neo-growth of mineral mass is valid for high supersaturations, it cannot explain the observations in nature of few and large crystals formed at low supersaturations, and many and small crystals at high supersaturations (e.g.,[16,103]), even if taking into account phenomena such as Ostwald ripening as crystals will eventually reach a local solubility that equals the bulk solubility.[104]

Starchenko et al.[70,105] studied the effect of fluid flow and reactions (Damköhler and Pe-numbers) using probabilistic nucleation−growth models. The formation of nucleation shadows at rapid reaction and low advective flow rates is particularly noteworthy. This phenomenon arises because solutes are depleted from regions adjacent to growing crystals.[105] Equally significant is the relative influence of nucleation and growth on the development of surface roughness.[70]

From a numerical performance point-of-view, the run-time penalty of adding mineral nucleation−growth to reactive transport simulations is considerable, especially if a full geochemical solver is used to estimate saturation states, pH, etc.[32] Earlier implementations were therefore limited to simplified geometry (e.g., 2D pore-scale[48,70,100,105]) and/or simplified geochemical systems (e.g., one component two phase system in Masoudi et al.[77]) In an effort to speed up complex 2D and 3D simulations, Peng et al. (2025)[32] developed an LB model coupled with an Artificial Neural Network (ANN) trained with geochemical data precalculated by the xGEMS code.[106−108] In addition to the novel combination of reactive transport with ANN, the model also included both a CNT-derived probabilistic model for the formation of crystalline phases and a deterministic nonclassical nucleation model for the formation of ACC.[32] This distinction is important for the present perspective, because it illustrates that ACC formation can be represented as a distinct precursor-forming step, while the appearance of crystalline polymorphs may additionally depend on subsequent ACC dissolution, ion transport, and phase-specific crystal growth. The efficiency gain from adding an ANN to the model was nearly 200,000-fold, indicating that future modeling with realistic 3D media, complex reactions, and even stochastic simulations running in parallel with the experiments is possible with the aid of machine-learning surrogates.

4. A MULTISITE, MULTIPOLYMORPH NUCLEATION MODEL

4.1. Intrinsic Surface Variability and Topography

There are differences in chemical reactivity of a crystal surface that arise solely from the solid material itself, particularly when its chemical composition and external environment, e.g., temperature, solution chemistry, and pH, are identical.[109] This variability originates from the atomic-scale architecture of the crystalline material, particularly its electronic structure.[110] Such local variations are highly significant for nanostructured surfaces, which frequently exhibit localized modifications in their surface electronic properties.[111]

Surface reactivity usually increases as atomic coordination decreases.[112] The overall variability in a solid material's reactivity is determined by its surface-atom coordination and local geometric arrangement. Surface atoms experience reduced coordination numbers and may exhibit unsatisfied (dangling) bonds or altered bond lengths and angles. This leads to a higher local chemical potential, enhanced adsorption strength, and lower activation barriers for reactions. Consequently, the kink and step sites of a crystal surface are the most reactive regions. Surface stress release at surface steps has been identified as the cause of inhomogeneous strain fields, which lead to distinct electronic structures and reactivity for terrace atoms with identical local coordination.[111]

Variations in electronic structure significantly influence adsorption reaction kinetics. Because surface atoms possess localized electronic states, adsorption energies fluctuate as a function of the local surface nanotopography. Numerical

Downloaded from pubs.acs.org/cgdefu/article-pdf/26/18/7321/6451959/acs.cgd.6c00312.pdf by guest on 19 October 2026

https://doi.org/10.1021/acs.cgd.6c00312
Cryst. Growth Des. 2026, 26, 7321−7336

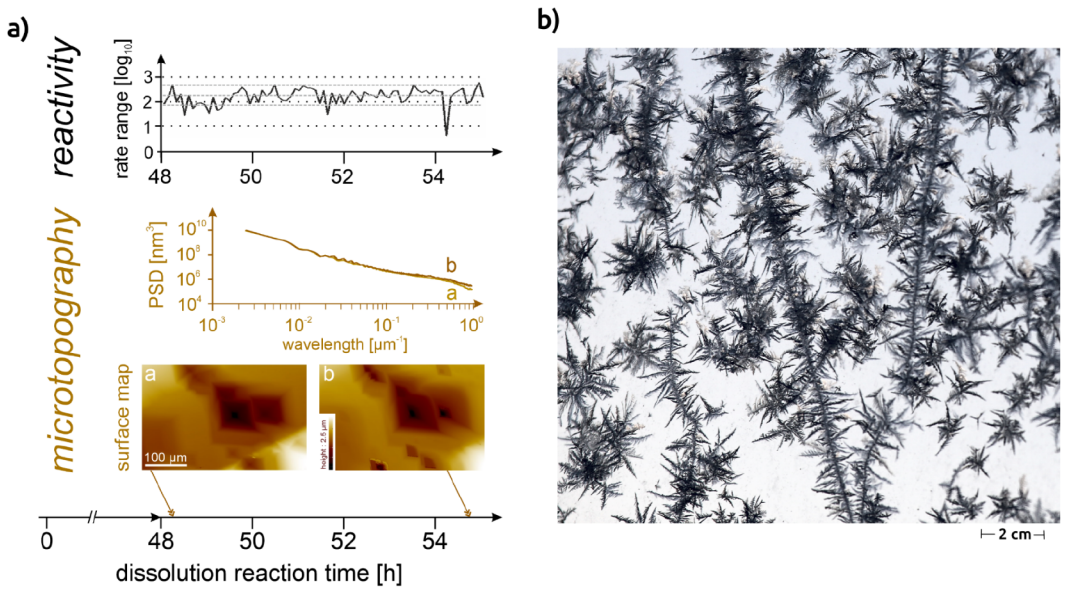


Figure 4. a) Surface reactivity and microtopography were monitored during a 7 h dissolution experiment following 48 h of prereaction to minimize preparation effects.[121] A total of 80 surface maps were collected using vertical scanning interferometry. Surface evolution is characterized by the growth of etch pits of different sizes. Changes in surface roughness across spatial scales were quantified using power spectral density (PSD) analysis (amber curves, averaged 1D PSD), showing similar PSD shapes at the beginning and end of the experiment, which indicates a steady-state surface with only minor shifts in the dominant surface features in the 1−300 μm range.[117,122] Dissolution rates and their variability were determined from difference maps of successive topographies (black curve). The rate variability remains stable at 2.2 ± 0.4 orders of magnitude throughout the experiment. b) Ice crystals on a glass panel. Imperfections in the surface lead to macroscopic nucleation patterns. We hypothesize that cross-scale PSD quantification possesses predictive capabilities and may serve as a robust metric for determining nucleation probability.

studies have compared and quantified the differences in the adsorption and desorption efficiencies of crystalline materials, providing a mechanistic explanation for related experimental observations.[113,114]

This effect is critical and decisive for nonideal, defect-bearing materials. Defects introduce the aforementioned constraints and define spatial importance (length and density) in crystalline materials. Although the consequences are observed in both crystal growth[115] and dissolution,[116] past analyses have focused on identifying the range of reactivity variability resulting from dissolution reactions, exemplified in Figure 4a: A single calcite crystal surface dissolution experiment under far-from-equilibrium conditions was performed to analyze reaction rate variability. The surface maps reveal the growth of etch pits of various sizes during the monitored reaction period. Power spectral density analysis indicates that the surface reached a steady-state condition, with only minor changes in the dominant spatial frequencies of the surface building blocks. The dissolution behavior observed over the 7 h reaction period exhibits a striking consistency: the variability in dissolution rates remains stable at 2.2 ± 0.4 orders of magnitude. Significantly, this stability reflects the persistence of the rate range rather than the mean rate. Despite this consistent variability, the shapes of the rate spectra, including their skewness, evolve markedly,[117] consistent with prior observations.[118] Beyond this illustrative case, various experimental and numerical studies have consistently identified a rate variability spanning two to 3 orders of magnitude. This range is not an artifact that vanishes as a system approaches steady state; rather, it is intrinsic to the steady state itself. This represents a dynamic equilibrium characterized by the continuous redistribution of surface sites and the ongoing evolution of topography at the nano- and microscale. While the spatial arrangement of these sites is in constant flux, the population density of specific site types, such as kink, step, and plateau sites, remains relatively stable. This behavior is captured by the rate spectrum,[119] which provides key insights into the functional consequences of heterogeneity in surface reactivity.[120]

Knowledge of the intrinsic rate variability is a prerequisite for predictive capabilities, as it persists even under transport-controlled conditions. Rather, it acts in combination with transport control and has recently been addressed in reactive transport modeling.[123,124]

An important question in crystal reaction kinetics is how reaction rates depend on Gibbs free energy (ΔG) as a system approaches or moves away from equilibrium. A related issue is whether rates are path-independent, that is, whether they are equivalent in both directions.

Dissolution experiments suggest a sigmoidal relationship between dissolution rate and saturation state. Far from equilibrium, rates are independent of ΔG, resulting in a dissolution plateau. Near equilibrium, rates decrease significantly and depend approximately linearly on saturation state. Two conclusions emerge from Atomic Force Microscopy (AFM) or Vertical Scanning Interferometry (VSI) studies.[125] First, different mechanisms dominate in different regimes. Near equilibrium, dissolution is mainly controlled by point defects and occurs without significant etch pit formation. Far from equilibrium, beyond a ΔG threshold, screw dislocations and step waves dominate, leading to rapid surface retreat. Second, surface topography inherited from previous reaction history strongly influences current kinetics. Crystals with identical bulk properties and experimental conditions can dissolve at markedly different rates, especially near equilibrium. Brief changes in ΔG that create or suppress etch pits can therefore exert long-lasting control on dissolution behavior. As a result, varying ΔG does not yield a stable intermediate steady-state

Downloaded from pubs.acs.org/cgdefu/article-pdf/26/18/7321/6451959/acs.cgd.6c00312.pdf by guest on 19 October 2026

https://doi.org/10.1021/acs.cgd.6c00312
Cryst. Growth Des. 2026, 26, 7321−7336

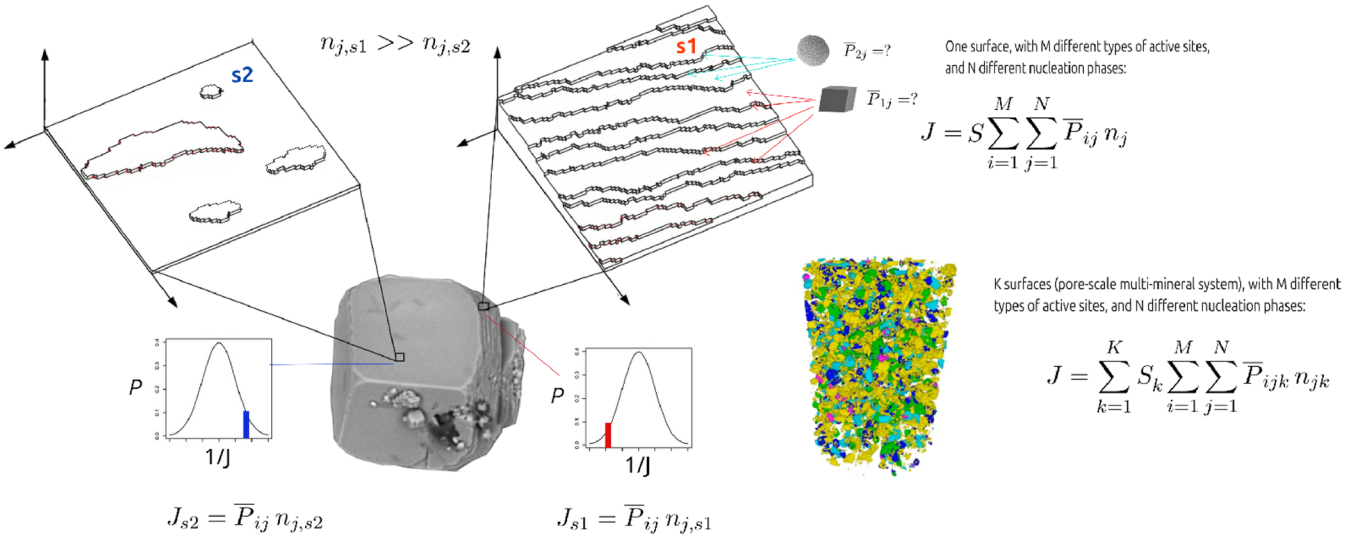


Figure 5. Macroscopic uncertainty in nucleation rates stems from the variety of surface reactivity due to different surface architectures, such as different densities of kinks and pits. These features are not seen by averaging nucleation models. Here illustrated with a calcite substrate with "flat" surfaces typically used for nucleation experiments, and curved or rough surfaces commonly found in realistic prereacted and reacting systems. J = integrated nucleation rate, $\overline{P}_{ij}$ = probability for nucleation of polymorph i on site j, n_j = number of active sites of type j.

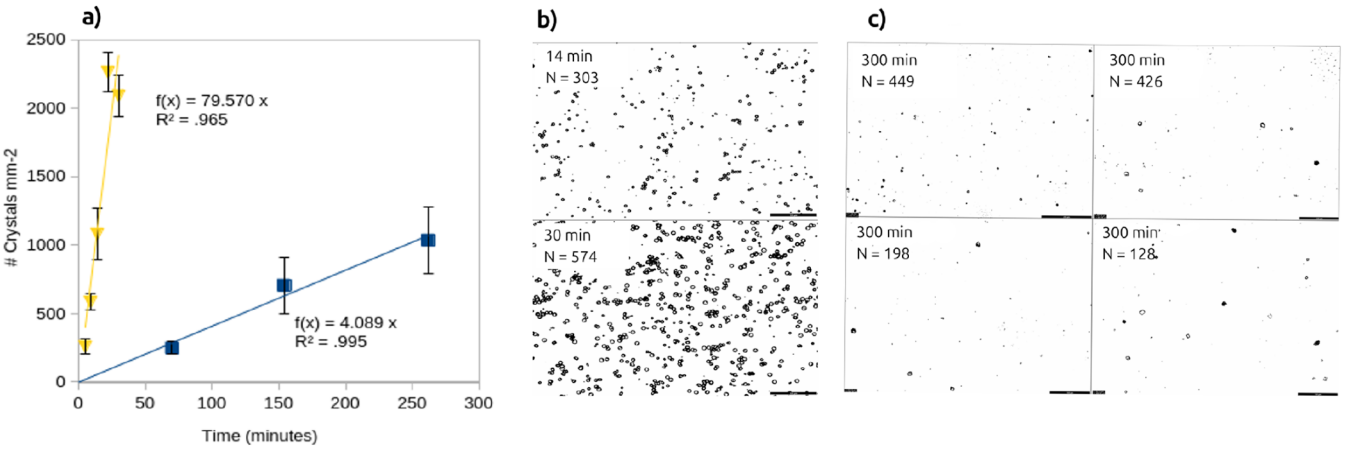


Figure 6. Preliminary experimental data for the nucleation of calcium carbonate on polished glass plates (48 × 28 × 1.35 mm Marienfeld plain microscope slides). Data obtained from reflection microscopy, and binary segmentation and crystal count done with the ImageJ/Fiji software.[131] a) Number of detected crystals with time at two supersaturations (about 30x and 170x). b) Each data point represents an individual experiment, sampled at different times. c) The error bars were estimated based on crystal counts on four different areas of one single experimental glass plate.

rate when transitioning between these mechanisms; instead, the observed rates are inherently nonsteady-state and history-dependent.

These insights are also relevant for nucleation and growth under supersaturated conditions. Topographically complex surfaces, particularly those previously affected by dissolution, have been shown to promote nucleation preferentially at step edges. Surface chemistry, topography, and charge act together to create effective nucleation sites and variable reaction rates.[46,47] The promoting effect of roughness has been demonstrated across a range of substrates, including scratched glass, structured silicon wafers, patterned PDMS, and even natural fibers.[126]

4.2. A Nanoscopic, Site-Resolved View of Nucleation Probabilities

The microscopic surface inherently features diverse site configurations, such as kinks, pits, and varying crystal orientations, which disrupt the macroscopically observed interfacial free energy. Consequently, nucleation is energetically favored at specific sites, where the probability of reaching the critical nucleus size is significantly enhanced (Figure 5). To estimate the total number of nuclei, n, formed on a surface, one must account for the population density of each site type, the site-specific nucleation probability, and the governing surface characteristics. The total number of nuclei, n, formed on a surface is given by the following expression:

$$n = S\Delta t \sum_{j=1}^{N} \overline{P}_{ij}\, n_j \tag{4}$$

where $\overline{P}_{ij}$ denotes the mean nucleation probability for polymorph i at site j (expressed as the long-run relative frequency in s^{-1}), n_j represents the density of site j per unit area, Δt is the time interval, and S is the total substrate surface area. The use of a mean value is justified by the large population of diverse surface sites present on a macroscopic surface. This equation remains valid provided that the site

https://doi.org/10.1021/acs.cgd.6c00312
Cryst. Growth Des. 2026, 26, 7321−7336

Downloaded from pubs.acs.org/cgdefu/article-pdf/26/18/7321/6645195/acs.cgd.6c00312.pdf by guest on 19 October 2026

densities and nucleation probabilities remain stationary over the defined time interval.

While the classical General Iterative Theory (GIT) model relies on the assumption of a stochastic process, it lacks empirical constraints for the standard deviation parameter ($\sigma = \tau_N/4$).[48,49] In contrast, the nanoscopic model presented in eq 4 is derived directly from the population of reactive sites, addressing the primary source of uncertainty in the macroscopic GIT model. Consequently, eq 4 provides a robust framework to constrain the probability density function employed in the GIT model. Preliminary experiments conducted on polished glass substrates (48 × 28 × 1.35 mm; Marienfeld microscope slides) under controlled conditions of temperature and calcium carbonate supersaturation support that, for identical substrates, the variation in nucleation rates and induction times remains minimal (Figure 6). These preliminary data are included as an illustrative proof of concept to support the proposed framework and its underlying assumptions.

When multiple amorphous or crystalline phases nucleate simultaneously from a supersaturated solution, the model must account for the nucleation probabilities of all phases across all reactive sites. Such multiphase competition is characteristic of systems such as calcium carbonate, where various transient amorphous and crystalline phases may emerge concurrently.[36,41,42] The total number of nuclei, n, for M possible phases is expressed as

$$n = S\Delta t \sum_{i=1}^{M} \sum_{j=1}^{N} \overline{P}_{ij}\, n_j \tag{5}$$

where the number of unique nucleus-substrate-site combinations expands to $N \times M$. Applying this multisite, multiphase probabilistic model to heterogeneous geological pore spaces necessitates the inclusion of additional surface areas, leading to the generalized expression:

$$n = \Delta t \sum_{k=1}^{K} S_k \sum_{i=1}^{M} \sum_{j=1}^{N} \overline{P}_{ijk}\, n_{jk} \tag{6}$$

In this formulation, K represents the number of distinct substrate surfaces, S_k is the total area of each surface k, and the total count of nucleus-substrate-site combinations becomes $N \times M \times K$. While this suggests a high dimensionality of parameters, a mechanistic understanding of these systems acts as a compass for mitigating uncertainties in nucleation and growth processes. Equations 4 through 6 demonstrate that while mean probabilities are sufficient at the microscopic scale, the primary uncertainty in predicting nucleation outcomes lies in the spatial distribution and density of surface sites. Because site distribution is largely a function of the solution saturation state, given that surface site densities remain temporally stable at constant temperature and chemistry,[117] these parameters are empirically accessible and, to a significant extent, predictable.

It is important to note that eq 5, and its generalization in eq 6, formulates polymorph selection as a set of parallel, site-specific nucleation probabilities. For calcium carbonate, however, a substantial body of evidence supports a nonclassical pathway in which ACC forms first and subsequently transforms into crystalline polymorphs through a path-dependent, solid-state or dissolution-reprecipitation process,[22,127−129] consistent with the precursor-phase formalism discussed in Section 2, in which ACC itself constitutes the metastable precursor phase. This is distinct from parallel, independent nucleation of each polymorph. At the same time, classical nucleation of crystalline polymorphs directly from solution has also been observed under specific thermodynamic and kinetic conditions,[57,128,130] and the relative importance of classical and nonclassical pathways, and the conditions under which each dominates, remains an active and unresolved debate in the literature. In our view, this question remains open and requires further investigation before a consensus can be reached. The framework presented here is therefore most directly applicable to systems and conditions in which parallel nucleation pathways dominate; extending it to path-dependent polymorph transformations, such as the ACC-to-crystalline transition, would require coupling the site-specific nucleation probabilities $\overline{P}_{ijk}$ to an additional transformation kinetics term describing the rate of internal structural rearrangement or desolvation of the precursor, analogous to the second step of the two-step nucleation formalisms introduced in Section 2.

Determining the probability for each nucleus-substrate-site pair through laboratory experiments and first-principles calculations is a complex challenge, as these values depend on numerous interdependent parameters. Both intrinsic (surface-related) and extrinsic (environmental) factors influence nucleation rates and dictate whether a classical or nonclassical pathway is followed. The substrate itself lowers the energy barrier for nucleation and may act as a template that preferentially stabilizes specific phases. Furthermore, the surface modifies the local fluid structure and near-surface chemical speciation within the diffuse double layer, while a nonuniform energy landscape can induce small-scale physical and chemical gradients. Surface orientation also explicitly influences the thermodynamic and kinetic affinity of a substrate. While crystalline substrates exhibit affinity heterogeneity through the aforementioned structural characteristics, amorphous substrates, such as glass, derive their heterogeneity from variations in local surface chemistry and topological disorder. Hierarchical materials, such as cement, present even greater complexity, as their surfaces are simultaneously heterogeneous, multiscale, and time-dependent. Extrinsic factors include the saturation state of the fluid with respect to the nucleating phase, the saturation state of the substrate (which influences the density of nucleation sites), and the ionic strength and pH, both of which affect saturation and the diffuse double layer. Additionally, parameters such as temperature, inhibitor concentrations, and even mechanical energy inputs, such as stirring, significantly influence the diffuse double layer and the immediate near-surface environment.

5. IMPLEMENTATION AND PARAMETRIZATION IN REACTIVE TRANSPORT MODELS

5.1. Scale of the Parameter Space

How do all these mentioned factors affect the nucleation pathway, the pre-exponential factor k_N, and the apparent interfacial free energy, and thereby $\overline{P}$? How can we obtain a useful data set that enables us to also predict with confidence nucleation−growth on a macro-scale, and how can a multisite polymorph-selective nucleation model be implemented in macroscopic reactive transport models? As noted earlier in this perspective, one reason for the lack of implementation of CNT, or any nucleation model, in reactive transport models is the absence of thermodynamic and kinetic parameters for heterogeneous nucleation.[83] This is certainly true, and the

Downloaded from pubs.acs.org/cgdefu/article-pdf/26/18/7321/6451959/acs.cgd.6c00312.pdf by guest on 19 October 2026

https://doi.org/10.1021/acs.cgd.6c00312
Cryst. Growth Des. 2026, 26, 7321−7336

question is then why a new multisite multiphase model, adding even more unknown parameters, can gain any traction in the scientific community. Even if such a model exists, how would it be possible to apply it in realistic cases where such parameters are typically a priori unknown or very difficult to determine?

The first question to address is the extent to which the new model complicates reactive transport modeling by introducing additional parameters. We can use an example. Following from eq 6, for a system with nucleation of two polymorphs on two different mineral surfaces, each with four distinct active sites, we will have to know $2 \times 2 \times 4 = 16$ different mean nucleation probabilities $\overline{P}_{ijk}$. If one of the phases is a precursor such as ACC, additional transformation, dissolution, or growth parameters may be required to describe the final crystalline polymorph distribution. This appears unmanageable if none of these 16 probability values are related, but this is unlikely.

For CNT, the interfacial free energy for heterogeneous nucleation can be estimated from the increased surface area between nuclei and solution and substrate (A_{nw} and A_{ns} respectively), and by subtracting the corresponding reduction of surface area between substrate and solution ($= A_{ns}$):

$$\Delta G^* = A_{nw}\sigma_{nw} + A_{ns}(\sigma_{ns} - \sigma_{sw}) \tag{7}$$

Steefel and van Cappellen[75] simplified expression 7 by assuming that the macroscopic energy barrier is solely a function of the newly created interface between the nucleus and solution (eliminating the nucleus-substrate and substrate solution interfacial tensions). This works well for a macroscopic, averaged model, but cannot be applied at the nanoscopic scale, as we must account for energy barriers at discrete surface sites. Equation 7 is in our opinion a very good starting point to bridge the microscopic and macroscopic scales. The removal of the substrate−solution interface at high σ_{sw} is the main reason for the reduction of the nucleation energy barrier and for the increased probability of nucleation at reactive sites. Since the footprint of a nucleus at critical size will normally extend beyond the reactive site itself, an integration of the surface tension over the nucleus footprint area will be required. This can be a straightforward task as long as the discrete site energies are known or can be computed for the relevant surface states, which is feasible for idealized crystalline substrate surfaces, but becomes challenging for evolving and chemically complex realistic surfaces. Discrete energy barriers can also be obtained from computational methods by estimating nucleation transition states at discrete sites.[43]

Once we have found the energy barrier for nucleation of one phase (e.g., vaterite) on all different surface sites, we can expect that the energy barrier for other phases (e.g., calcite) will be related to the former, since the energy barrier of all nucleating phases will all share the same discrete interfacial tension component of the surface sites. This argument applies most directly to crystalline phases nucleating competitively from solution. For such a system, the ACC-mediated pathways require an additional description of the precursor state and its subsequent transformation, dissolution, or coupling to crystalline growth.

The second is to find the number of each surface site type (n_{jk} in eq 6). These numbers will depend strongly on the saturation state of the solution with respect to the surface and to a lesser extent the background chemical composition and the prior long-term reaction history, since surfaces tend to form a dynamic equilibrium after a fairly short time (hours-days for CC)[117] (see Section 4.1).

Once the transition states for each site are determined and the population density of these discrete sites is estimated, macroscopic nucleation rates can be derived deterministically. Although incorporating these microscopic features introduces additional variables not required by traditional macroscopic probabilistic models, this approach is justified. By accounting for the specific physical variables that drive stochasticity, this multisite, polymorph-selective model provides a framework for quantifying and explaining macroscopic uncertainty. In practice, the primary challenge is not the model itself but the efficient acquisition and inference of these microparameters across heterogeneous, evolving surfaces under diverse chemical conditions. These challenges may be effectively addressed through the integration of advanced experimental and computational modeling techniques.

5.2. Role of Machine Learning and AI in Model Parametrization

It is clear that for realistic systems, eq 6 will have a large number of degrees of freedom and of unknown parameters, including mean nucleation probabilities P_{ijk}, site densities n_{jk}, kinetic prefactors, and effective interfacial-energy-related quantities for different combinations of polymorph i, site type j, and substrate k.

Some parameters may be correlated; however, carefully designed experiments can allow the extraction of universal, transferable results across systems. In such a high-dimensional space, traditional approaches will be very challenging to apply. However, machine learning (ML), Artificial Intelligence (AI) and automation can play a significant role in parametrizing and deploying the proposed multisite multiphase model by a) supporting the design of experimental setups b) enhancing the processing of the experimental results c) steering experiments and autonomously exploring the parameter space, d) enabling parameter inference and uncertainty quantification for the quantities entering eq 6, and e) accelerating by several orders of magnitude the reactive transport codes to be used for inverse modeling of the experiments, sensitivity analysis and uncertainty quantification. Thus, AI/ML can play an enabling role in several distinct yet connected tasks: experimental design, automated data extraction, autonomous experimental steering, parameter inference, and reactive transport simulation acceleration. At the same time, the AI/ML role is not to replace the mechanistic nucleation model, but as an enabling framework for calibrating, constraining, and deploying it at the reactive transport modeling scale.

The role of ML is crucial for the *design of experiments* when experimental outcomes depend on multiple interacting parameters and nonlinear mechanisms. Careful design of experimental campaigns is essential to minimize the number of required investigations while maximizing knowledge gain, and initial experimental configurations can be guided by domain expertise. Subsequent experiments can then be adaptively selected based on information gained from earlier results, using active learning and sequential decision-making strategies subject to physics-informed constraints, thereby enabling efficient and physically consistent exploration of the parameter space. Within the scope of experimental parametrization, the boundary conditions that define mixture concentrations will need to be explored, along with variable substrate surface treatments. The output of this approach can therefore be an optimized experimental campaign that targets the most informative regions of the parameter space relevant to eq 6,

Downloaded from pubs.acs.org/cgdefu/article-pdf/26/18/7321/6645195/acs.cgd.6c00312.pdf by guest on 19 October 2026

https://doi.org/10.1021/acs.cgd.6c00312
Cryst. Growth Des. 2026, 26, 7321−7336

rather than a replacement of the nucleation model. A key challenge will be the data efficiency, since nucleation experiments can be slow, stochastic, and sensitive to surface preparation. In this regard, active-learning and Bayesian-optimization strategies may account for experimental noise, induction time distributions, and nucleation probabilities.

At the same time, ML/AI can enable and support high-dimensional *experimental investigations*. Exploring such a vast parameter space requires a rethinking of conventional experimental setups. Miniaturized experiments must be designed using micromachining and microfluidic technologies to be executed in parallel, particularly when statistically meaningful quantities, such as induction time distributions and nucleation probabilities, are required. An example of this approach, in which a large number of microdroplet experiments were analyzed on a single microfluidic multiphase chip, was reported in ref 132. This allowed the simultaneous investigation of the dependence of Barite nucleation on induction time and pore size. The analysis of such experiments, which typically involve the temporal evolution of hundreds to thousands of droplet microreactors, is greatly facilitated by AI-based methods, such as computer vision. Automated history recording and detection of crystallization events within individual microdroplets enable the extraction of probabilistic nucleation statistics.[133,134] In the context of a multiparameter model, such workflows may directly target the key inputs of eq 6 if adapted to account for substrate heterogeneity and multispecies interactions. In this context, AI/ML acts primarily as an automated data-extraction tool, converting images, videos, and time-resolved experimental records into nucleation observables such as induction-time distributions, nucleation probabilities, and their dependence on substrate and solution compositions. These observables then provide the data basis for estimating or constraining the parameters of eq 6, including P_{ijk}, kinetic coefficients, and interfacial energy-related quantities.

In neighboring disciplines *autonomous experimental investigations* of chemical systems and pathways have started to emerge. Such an example is the seminal work of Martin et al.,[135] where the autonomous formulation lab technology was deployed to explore a vast parameter space, aiming to accelerate the discovery of liquid formulations for specific applications. At the same time, it has been shown that the discovery cycle can also be accelerated by combining AI, robotics, and high-performance computing, as reported in ref 136, in the discovery of novel chemically amplified photoresist materials for micro- and nanoelectronics manufacturing applications. Related conceptual elements have been discussed in the context of geochemical discovery problems, including the theoretical net-zero cement formulation design.[137] These examples illustrate the potential of autonomous and AI-assisted discovery workflows for steering experiments and exploring parameter spaces with respect to the overall objective of mechanistic understanding of nucleation processes.

The resulting knowledge gain can be postprocessed and modeled using machine learning encoding and decoding to establish a link between experimental observations and the theoretical modeling approach. This parameter extraction step may rely on Bayesian calibration, probabilistic ML, Gaussian process regression, neural network-based regressors, or hybrid approaches that combine mechanistic constraints with data-driven components.[138−140] This approach not only aims to provide *best-fit parameters* but also to quantify *parameter uncertainty*, correlations, and transferability across substrates, mineral phases, and chemical conditions. A limitation of microfluidic platforms is that the substrate geometry, heterogeneity, and surface chemistry may be simplified compared with what is observed in natural porous media. Therefore, parameters inferred from such experiments should be validated against more complex substrates, and, where necessary, supported by surface characterization.

Finally, AI and ML techniques can be used to significantly *accelerate numerical solvers* and enable advanced sensitivity analysis, uncertainty quantification, and inverse modeling workflows that would otherwise be computationally prohibitive. This is especially important for multiscale, multiphysics nucleation and reactive-transport models. At a first level of individual processes, data-driven surrogate models can approximate high-fidelity solvers at a fraction of the computational cost, enabling efficient exploration of high-dimensional parameter spaces and probabilistic inference of poorly constrained quantities such as nucleation rates, site densities, and interfacial energies. For reactive transport, it has been shown that a two- to four-orders of magnitude speed up of the simulation code, without loss of accuracy, can be achieved by creating machine learning based surrogate models of the thermodynamics and involved chemistry.[141−143] Prominent models are typically based on neural network machine learning, in which the training and test data sets are generated by the respective geochemical and thermodynamic speciation solvers. At the level of the reactive transport simulation, it is possible to encode the physics in machine learning models to enable fast inference[144] and support inverse modeling of the experiments. Emerging methods, including physics-informed neural networks[145] and operator learning approaches,[146] remain underexplored. In the context of the present discussion, such operator-learning approaches should be understood as possible future surrogate or simulation acceleration strategies, especially for simulations involving evolving pore geometries, rather than as a separate replacement for the mechanistic nucleation model. A critical limitation of surrogate accelerated reactive transport simulations is that small surrogate errors may accumulate over many time steps, potentially leading to simulation drift, mass-balance errors, or unphysical concentration trajectories. Therefore, highly accurate surrogates, error monitoring, and validation against the full geochemical or reactive transport solver are essential elements of such workflows.

Together, these methods enable fast-forward models, gradient-based sensitivity analysis, and uncertainty propagation analysis. Crucially, all the aforementioned AI/ML techniques can greatly enable and support, but certainly not replace, the mechanistic nucleation modeling by making the calibration, sensitivity analysis, and uncertainty propagation feasible for eq 6 at the reactive transport modeling scale.

6. CONCLUSIONS

This perspective has argued that the large uncertainties commonly reported for macroscopic nucleation rates are not merely stochastic noise to be averaged away, but largely reflect the nanoscale heterogeneity of the substrate surface itself. Surfaces that appear macroscopically identical can differ substantially in the density and nature of their active sites, kinks, steps, terraces, and defects, as a result of distinct physical or chemical alteration histories, crystallographic orientations, or impurity contents. Once quantified, these nanoscopic

Downloaded from pubs.acs.org/cgdefu/article-pdf/26/18/7321/6451959/acs.cgd.6c00312.pdf by guest on 19 October 2026

https://doi.org/10.1021/acs.cgd.6c00312
Cryst. Growth Des. 2026, 26, 7321−7336

differences can be related directly to the macroscopic variations and uncertainties observed experimentally, while the remaining fast, stochastic atomistic processes can continue to be treated statistically.

Realizing this connection, even for simple systems, will require a collective effort that combines first-principles calculations with laboratory experiments and new upscaling schemes capable of capturing the "invisible" variations that macroscopic models currently miss. We expect such an effort to yield not only system-specific knowledge but also more broadly transferable insight, for instance, into how the relative reduction of nucleation barriers at different active surface sites compares across mineral systems.

The main conclusions of this perspective are as follows:

- The multisite, multipolymorph nucleation framework proposed here (eqs 4-6) replaces the averaged interfacial free energy of classical nucleation theory with an explicit sum over site-specific nucleation probabilities $\overline{P}_{ijk}$ and site densities n_{jk}. This reformulation grounds the probability density functions used in existing macroscopic probabilistic models in measurable, physically meaningful quantities, and provides a basis for explaining, rather than merely fitting, the observed uncertainty in macroscopic nucleation rates.
- The reactivity of natural and synthetic surfaces exhibits intrinsic, quantifiable variability, evidenced by dissolution rate spectra. This variability can be related, at least in part, to defect type and density, reaction history, and crystallographic orientation, providing a quantitative and spatial basis for the site densities n_{jk} required by the proposed framework.
- The role of heterogeneous nucleation in polymorph selection remains an open question. For calcium carbonate, both parallel nucleation of distinct polymorphs and path-dependent transformation from an amorphous precursor have been documented, and which pathway dominates under given conditions remains debated. For ACC-mediated calcium carbonate systems, polymorph selection may additionally be path-dependent, requiring precursor formation, stabilization, dissolution, ion transport, and crystalline growth to be described in addition to parallel nucleation probabilities.
- Machine learning offers a coherent set of tools for making the proposed framework tractable: active learning and automated experimental design for efficiently constraining $\overline{P}_{ijk}$ and n_{jk}, computer vision for high-throughput extraction of nucleation statistics, surrogate models for accelerating reactive transport simulations by orders of magnitude, and neural operators for efficient forward simulation across evolving pore geometries. These tools support but do not replace the mechanistic understanding provided by the proposed framework.

Taken together, these conclusions outline a path from nanoscopic surface characterization to deterministic, physically grounded predictions of macroscopic nucleation rates. While the parameter space remains large, the combination of a mechanistic multisite framework with modern experimental and computational tools makes this path tractable, and we anticipate that pursuing it will substantially improve our ability to predict mineral nucleation in coupled reactive transport systems.

AUTHOR INFORMATION

Corresponding Author

Helge Hellevang − *Department of Geosciences, University of Oslo, Oslo 0316, Norway;* orcid.org/0009-0004-6409-7849; Email: helge.hellevang@geo.uio.no

Authors

Cornelius Fischer − *Institut für Ressourcenökologie, Helmholtz-Zentrum Dresden-Rossendorf (HZDR) & Institut für Anorganische Chemie, Universität Leipzig, 04103 Leipzig, Germany;* orcid.org/0000-0003-2416-6438

Mohammad Nooraiepour − *Department of Geosciences, University of Oslo, Oslo 0316, Norway;* orcid.org/0000-0003-3466-5783

Sergi Molins − *Earth and Environmental Sciences Area, Lawrence Berkeley National Laboratory, Berkeley, California 94720, United States;* orcid.org/0000-0001-7675-3218

Mohammad Masoudi − *Applied Geoscience Department, SINTEF Industry, Trondheim 7465, Norway;* orcid.org/0000-0001-6560-0400

Nikolaos I. Prasianakis − *PSI Center for Nuclear Engineering and Sciences, Villigen PSI 5232, Switzerland*

Complete contact information is available at: https://pubs.acs.org/10.1021/acs.cgd.6c00312

Notes

The authors declare no competing financial interest.

ACKNOWLEDGMENTS

H.H. and M.N. acknowledge support from the Norwegian Centennial Chair Program through the project "Carbon Mineralization in Basaltic Rocks—Understanding Coupled Mineral Dissolution and Precipitation in Reactive Subsurface Environments." M.N. and M.M. acknowledge support from the Research Council of Norway through the Multiphysics of Salt Precipitation During CO_2 Storage (Saltation) project, project number 357784.

REFERENCES

(1) White, C. E.; Provis, J. L.; Proffen, T.; van Deventer, J. S. J. Molecular mechanisms responsible for the structural changes occurring during geopolymerization: Multiscale simulation. *AIChE J.* **2012**, *58* (7), 2241−2253.

(2) Provis, J. L.; Hajimohammadi, A.; White, C. E.; Bernal, S. A.; Myers, R. J.; Winarski, R. P.; Rose, V.; Proffen, T. E.; Llobet, A.; van Deventer, J. S. Nanostructural characterization of geopolymers by advanced beamline techniques. *Cem. Concr. Compos.* **2013**, *36*, 56−64. Special issue: Nanotechnology in Construction

(3) John, E.; Lothenbach, B. Cement hydration mechanisms through time−a review. *J. Mater. Sci.* **2023**, *58*, 9805−9833.

(4) Qianqian, L.; Chunyu, D.; Bin, S.; Pengjian, Z.; Xinqun, C.; Yulin, M.; Geping, Y.; Gao, Y. Understanding undesirable anode lithium plating issues in lithium-ion batteries. *R. Soc. Chem. Adv.* **2016**, *6*, 88683−88700.

(5) Thirumalraj, B.; Hagos, T. T.; Huang, C.-J.; Teshager, M. A.; Cheng, J.-H.; Su, W.-N.; Hwang, B.-J. Nucleation and Growth Mechanism of Lithium Metal Electroplating. *J. Am. Chem. Soc.* **2019**, *141* (46), 18612−18623.

(6) Abbas, S. M.; Gstrein, G.; Jauernig, A. D.; Schmid, A.; Michelini, E.; Hinterberger, M.; Ellersdorfer, C. Influence of Lithium Plating on the Mechanical Properties of Automotive High-Energy Pouch Batteries. *Batteries* **2025**, *11* (9), 330.

(7) Drioli, E.; Di Profio, G.; Curcio, E. Progress in membrane crystallization. *Curr. Opin. Chem. Eng.* **2012**, *1* (2), 178−182.

Downloaded from pubs.acs.org/cgdefu/article-pdf/26/18/7321/6451959/acs.cgd.6c00312.pdf by guest on 19 October 2026

(8) Quist-Jensen, C.; Macedonio, F.; Drioli, E. Membrane crystallization for salts recovery from brine—an experimental and theoretical analysis. *Desalin. Water Treat.* **2016**, *57* (16), 7593−7603.
(9) Shen, L.; Dang, M.; Han, X. Recent advances in membrane crystallization. *CrystEngComm* **2023**, *25*, 2503−2517.
(10) Baker, R. *Membrane Technology and Applications*, ISBN: 978−0-470−74372−0; Wiley, 2012.
(11) Nassr, M.; Dischinger, S. M.; Lee, J. Y.; Gleason, K. L.; Molins, S.; Spycher, N.; Bigdelou, P.; Johnston, J.; Lynd, N. A.; Tilton, N.; Stringfellow, W. T.; Freeman, B. D.; Miller, D. J. Mineral Scale Formation during Crossflow Reverse Osmosis at Constant Flux and Constant Transmembrane Pressure Conditions. *Ind. Eng. Chem. Res.* **2025**, *64* (2), 1295−1308.
(12) Olajire, A. A. A review of oilfield scale management technology for oil and gas production. *J. Pet. Sci. Eng.* **2015**, *135*, 723−737.
(13) Kumar, R.; Li, M.; Munday, L. B.; Simmons, S.; Smith, R.; Neupane, G.; Colldeweih, R.; Mcling, T.; Podgorney, R.Estimating Mineral Scaling and Porosity Alterations During the Circulation Test at Utah-FORGE Site Using Reactive Transport Modeling en. In*50th Workshop On Geothermal Reservoir Engineering*; Stanford University: Stanford, CA, USA, Feb. 2025
(14) Pátzay, G.; Stáhl, G.; Kármán, F.; Kálmán, E. Modeling of scale formation and corrosion from geothermal water. *Electrochim. Acta* **1998**, *43* (1), 137−147. Corrosion
(15) Pham, V.; Lu, P.; Aagaard, P.; Zhu, C.; Hellevang, H. On the potential of CO2−water−rock interactions for CO2 storage using a modified kinetic model. *Int. J. Greenhouse Gas Control.* **2011**, *5* (4), 1002−1015.
(16) Miri, R.; van Noort, R.; Aagaard, P.; Hellevang, H. New insights on the physics of salt precipitation during injection of CO2 into saline aquifers. *Int. J. Greenhouse Gas Control.* **2015**, *43*, 10−21.
(17) Miri, R.; Hellevang, H. Salt precipitation during CO2 storage—A review. *Int. J. Greenhouse Gas Control.* **2016**, *51*, 136−147.
(18) Nooraiepour, M.; Fazeli, H.; Miri, R.; Hellevang, H. Effect of CO2 phase states and flow rate on salt precipitation in shale caprocks—a microfluidic study. *Environ. Sci. Technol.* **2018**, *52* (10), 6050−6060.
(19) Nooraiepour, M.; Masoudi, M.; Derluyn, H.; Senechal, P.; Moonen, P.; Hellevang, H. Halite Precipitates as Porous Crystalline Networks, Not Dispersed Crystals: Self-Enhancing Growth Mechanisms During CO2 Storage in Saline Aquifers. *Chem. Eng. J.* **2026**, *543*, 178165.
(20) Gebauer, D.; Völkel, A.; Cölfen, H. Stable Prenucleation Calcium Carbonate Clusters. *Science* **2008**, *322*, 1819−1822.
(21) Sleuter, M.; Lutsko, J.; Van Driessche, A. E.; Durán-Olivencia, M. A.; Maes, D. Observing classical nucleation theory at work by monitoring phase transitions with molecular precision. *Nat. Commun.* **2014**, *5* (1), 5598.
(22) De Yoreo, J.Chapter 1: A Perspective on Multistep Pathways of Nucleation*Crystallization Via Nonclassical Pathways Volume 1: nucleation, Assembly, Observation Application*American Chemical Society (ACS)2020*13*581−17
(23) Jun, Y.-S.; Zhu, Y.; Wang, Y.; Ghim, D.; Wu, X.; Kim, D.; Jung, H. Classical and Nonclassical Nucleation and Growth Mechanisms for Nanoparticle Formation. *Annu. Rev. Phys. Chem.* **2022**, *73*, 453−477.
(24) Darkins, R.; Duffy, D. M.; Ford, I. J. Prenucleation Cluster Pathway is Inconsistent with CaCO3 Kinetics. *Cryst. Growth Des.* **2024**, *24* (10), 4013−4016.
(25) Nooraiepour, M.; Masoudi, M.; Hellevang, H. Carbon Mineralization in CO2−Seawater−Basalt Systems: Reactive Transport Dynamics and Vesicular Pore Architecture Controls. *Langmuir* **2026**, *42*, 11435−11456.
(26) Gebauer, D.; Kellermeier, M.; Gale, J. D.; Bergström, L.; Cölfen, H. Pre-nucleation clusters as solute precursors in crystallisation. *Chem. Soc. Rev.* **2014**, *43*, 2348−2371.
(27) Smeets, P. J. M.; Finney, A. R.; Habraken, W. J. E. M.; Nudelman, F.; Friedrich, H.; Laven, J.; Yoreo, J. J. D.; Rodger, P. M.; Sommerdijk, N. A. J. M. A classical view on nonclassical nucleation. *Proc. Natl. Acad. Sci. U. S. A.* **2017**, *114* (38), No. E7882−E7890.
(28) Vekilov, P. G. Dense Liquid Precursor for the Nucleation of Ordered Solid Phases from Solution. *Cryst. Growth Des.* **2004**, *4* (4), 671−685.
(29) Xu, Y.; Tijssen, K. C. H.; Bomans, P. H. H.; Akiva, A.; Friedrich, H.; Kentgens, A. P. M.; Sommerdijk, N. A. J. M. Microscopic structure of the polymer-induced liquid precursor for calcium carbonate. *Nat. Commun.* **2018**, *9*, 2582.
(30) Stawski, T. M.; Salvalaglio, M.; Wallace, A. F.; De Yoreo, J. J. The Birth of Minerals: From Single Step to Multiple Step Mechanisms. *Elements* **2025**, *21* (1), 25−32.
(31) Li, C.; Goonetilleke, E. C.; Huang, X.; Huang, X. Temperature-dependent kinetic pathways of heterogeneous ice nucleation competing between classical and non-classical nucleation. *Nat. Commun.* **2021**, *12* (1), 4954.
(32) Peng, H.; Rajyaguru, A.; Curti, E.; Grolimund, D.; Churakov, S. V.; Prasianakis, N. I. Machine Learning-Enhanced Modeling of Calcium Carbonate Nucleation in Porous Media Under Counter-Diffusion Conditions. *Water Resour. Res.* **2025**, *61* (11), No. e2025WR040484.
(33) Aradóttir, E. S.; Sigurdardóttir, H.; Sigfússon, B.; Gunnlaugsson, E. CarbFix: A CCS pilot project imitating and accelerating natural CO2 sequestration. *Greenhouse Gases: sci. Technol.* **2011**, *1* (2), 105−118.
(34) Teng, H.; Dove, P. M.; De Yoreo, J. J. Kinetics of calcite growth: Surface processes and relationships to macroscopic rate laws. *Geochim. Cosmochim. Acta* **2000**, *64* (13), 2255−2266.
(35) Berner, R. The long-term carbon cycle, fossil fuels and atmospheric composition. *Nature* **2003**, *426*, 323−326.
(36) Nielsen, M. H.; Aloni, S.; Yoreo, J. J. D. In situ TEM imaging of $CaCO_3$ nucleation reveals coexistence of direct and indirect pathways. *Science* **2014**, *345* (6201), 1158−1162.
(37) Wang, Y.; Zeng, M.; Meldrum, F. C.; Christenson, H. K. Using Confinement To Study the Crystallization Pathway of Calcium Carbonate. *Cryst. Growth Des.* **2017**, *17* (12), 6787−6792.
(38) Avaro, J. T.; Wolf, S. L. P.; Hauser, K.; Gebauer, D. Stable Prenucleation Calcium Carbonate Clusters Define Liquid−Liquid Phase Separation. *Angew. Chem., Int. Ed.* **2020**, *59* (15), 6155−6159.
(39) Di Lorenzo, F.; Steiner, K.; Churakov, S. V. The Effect of pH, Ionic Strength and the Presence of PbII on the Formation of Calcium Carbonate from Homogenous Alkaline Solutions at Room Temperature. *Minerals* **2021**, *11* (7), 783.
(40) Meldrum, F.; Cölfen, H. The many lives of calcium carbonate. *Nat. Chem.* **2023**, *15*, 1196.
(41) Stolarski, J.; van Dijk, I.; Benning, L. G. Controls on CaCO3 Polymorphism: From Laboratory Precipitation to Biomineralization across Geological Time. *Elements* **2025**, *21* (2), 92−97.
(42) Bots, P.; Benning, L.; Rickaby, R.; Shaw, S. The role of SO4 in the switch from calcite to aragonite seas. *Geology* **2011**, *39* (4), 331−334.
(43) Bulutoglu, P. S.; Zalte, A. S.; Nere, N. K.; Ramkrishna, D.; Corti, D. S. A comprehensive modeling approach for polymorph selection in Lennard-Jones crystallization. *J. Chem. Phys.* **2023**, *158* (13), 134505.
(44) Stenzel, H.; Bethge, H. An investigation of heterogeneous nucleation on point defects. *Thin Solid Films* **1976**, *32* (2), 267−270.
(45) Cardoso, J.; Harsdorff, M. The Influence of Surface Defects on the Heterogeneous Nucleation and Growth of Thin Films. *Z. Naturforsch. A* **1978**, *33* (4), 442−446.
(46) Campbell, J. M.; Meldrum, F. C.; Christenson, H. K. Characterization of Preferred Crystal Nucleation Sites on Mica Surfaces. *Cryst. Growth Des.* **2013**, *13* (5), 1915−1925.
(47) Dunn, T. H.; Skaanvik, S. A.; McPherson, I. J.; O'Shaughnessy, C.; He, X.; Kulak, A. N.; Micklethwaite, S.; Matamoros-Veloza, A.; Sandei, I.; Hunter, L.; Turner, T. D.; Galloway, J. M.; Rosenthal, M.; Britton, A. J.; Walker, M.; Dong, M.; Unwin, P. R.; Meldrum, F. C. Universality of Hair as a Nucleant: Exploring the Effects of Surface Chemistry and Topography. *Cryst. Growth Des.* **2023**, *23* (12), 8978−8990.

Downloaded from pubs.acs.org/cgdefu/article-pdf/26/18/7321/6451959/acs.cgd.6c00312.pdf by guest on 19 October 2026

https://doi.org/10.1021/acs.cgd.6c00312
Cryst. Growth Des. 2026, 26, 7321−7336

(48) Fazeli, H.; Masoudi, M.; Patel, R. A.; Aagaard, P.; Hellevang, H. Pore-Scale Modeling of Nucleation and Growth in Porous Media. *ACS Earth Space Chem.* **2020**, *4* (2), 249−260.
(49) Nooraiepour, M.; Masoudi, M.; Hellevang, H. Probabilistic nucleation governs time, amount, and location of mineral precipitation and geometry evolution in the porous medium. *Sci. Rep.* **2021**, *11* (1), 16397.
(50) Zhang, J.; Nancollas, G. H. Kink Density and Rate of Step Movement during Growth and Dissolution of an AB Crystal in a Nonstoichiometric Solution. *J. Colloid Interface Sci.* **1998**, *200* (1), 131−145.
(51) Wolthers, M.; Nehrke, G.; Gustafsson, J. P.; Van Cappellen, P. Calcite growth kinetics: Modeling the effect of solution stoichiometry. *Geochim. Cosmochim. Acta* **2012**, *77*, 121−134.
(52) Hellevang, H.; Miri, R.; Haile, B. G. New Insights into the Mechanisms Controlling the Rate of Crystal Growth. *Cryst. Growth Des.* **2014**, *14* (12), 6451−6458.
(53) Hellevang, H.; Haile, B. G.; Miri, R. A Statistical Approach To Explain the Solution Stoichiometry Effect on Crystal Growth Rates. *Cryst. Growth Des.* **2016**, *16* (3), 1337−1348.
(54) Seepma, S. Y. M. H.; Ruiz-Hernandez, S. E.; Nehrke, G.; Soetaert, K.; Philipse, A. P.; Kuipers, B. W. M.; Wolthers, M. Controlling CaCO3 Particle Size with Ca2+: CO32− Ratios in Aqueous Environments. *Cryst. Growth Des.* **2021**, *21* (3), 1576−1590.
(55) Peters, V. F. D.; Baken, A.; Seepma, S. Y. M. H.; Koskamp, J. A.; Fernández-Martínez, A.; van Driessche, A. E. S.; Wolthers, M. Effect of Solution Stoichiometry on BaSO4 Crystallization from Turbidity Measurements and Modeling. *Ind. Eng. Chem. Res.* **2024**, *63* (1), 78−88.
(56) Koskamp, J. A.; Seepma, S. Y. M. H.; Peters, V. F. D.; Toroz, D.; Di Tommaso, D.; Wolthers, M. The impact of stoichiometry on the initial steps of crystal formation: Stability and lifetime of charged triple-ion complexes. *Chem. Eur. J.* **2024**, *30* (20), No. e202303860.
(57) Gebauer, D.; Raiteri, P.; Gale, J. D.; Cölfen, H. On classical and non-classical views on nucleation. *Am. J. Sci.* **2018**, *318* (9), 969−988.
(58) Zahn, D. Thermodynamics and kinetics of prenucleation clusters, classical and non-classical nucleation. *ChemPhysChem* **2015**, *16* (10), 2069−2075.
(59) Durán-Olivencia, M. A.; Yatsyshin, P.; Kalliadasis, S.; Lutsko, J. F. General framework for nonclassical nucleation. *New J. Phys.* **2018**, *20* (8), 083019.
(60) Erdemir, D.; Lee, A. Y.; Myerson, A. S. Nucleation of crystals from solution: Classical and two-step models. *Acc. Chem. Res.* **2009**, *42* (5), 621−629.
(61) Kashchiev, D.; Vekilov, P. G.; Kolomeisky, A. B. Kinetics of two-step nucleation of crystals. *J. Chem. Phys.* **2005**, *122* (24), 244706.
(62) Gebauer, D.; Cölfen, H. Prenucleation clusters and non-classical nucleation. *Nano Today* **2011**, *6* (6), 564−584.
(63) Volmer, M. ÜBer Keimbildun Und Keimwirkung Als SpezialfÄlle Der Heterogenen Katalyse. *Z. Elektrochem. Angew. Phys. Chem.* **1929**, *35* (9), 555−561.
(64) Becker, R.; Döring, W. Kinetische Behandlung der Keimbildung in übersättigten Dämpfen. *Ann. Phys.* **1935**, *416* (8), 719−752.
(65) Volmer, M. Kinetik der Phasenbildung. *Chemische Reaktion*; Steinkopff, 1939.
(66) Frenkel, Y. *Kinetic theory of liquids*; Oxford University Press: London, 1946.
(67) Pound, G. M.; Mer, V. K. L. Kinetics of Crystalline Nucleus Formation in Supercooled Liquid Tin1,2. *J. Am. Chem. Soc.* **1952**, *74* (9), 2323−2332.
(68) Toschev, S.; Milchev, A.; Stoyanov, S. On some probabilistic aspects of the nucleation process. *J. Cryst. Growth* **1972**, *13*−*14*, 123−127. Third International Conference on Crystal Growth
(69) Curcio, E.; Di Profio, G.; Drioli, E. Probabilistic aspects of polymorph selection by heterogeneous nucleation on microporous hydrophobic membrane surfaces. *J. Cryst. Growth* **2008**, *310* (24), 5364−5369.
(70) Starchenko, V. Pore-Scale Modeling of Mineral Growth and Nucleation in Reactive Flow. *Front. Water.* **2022**, *3*, 800944.
(71) Zeldovich, Y. B. On the theory of new phase formation. Cavitation. *Zh. Eksp. Teor. Fiz.* **1942**, *12*, 525−538.
(72) Steefel, C. I.; De Paolo, D. J.; Lichtner, P. C. Reactive transport modeling: An essential tool and a new research approach for the Earth sciences. *Earth Planet. Sci. Lett.* **2005**, *240* (3−4), 539−558.
(73) Seigneur, N.; Mayer, K. U.; Steefel, C. I. Reactive Transport in Evolving Porous Media. *Rev. Mineral. GeoChem* **2019**, *85* (1), 197−238.
(74) Noiriel, C.; Soulaine, C. Pore-Scale Imaging and Modelling of Reactive Flow in Evolving Porous Media: Tracking the Dynamics of the Fluid−Rock Interface. *Transp. Porous Media* **2021**, *140*, 181−213.
(75) Steefel, C. I.; Van Cappellen, P. A new kinetic approach to modeling water-rock interaction: The role of nucleation, precursors, and Ostwald ripening. *Geochim. Cosmochim. Acta* **1990**, *54* (10), 2657−2677.
(76) Noiriel, C.; Seigneur, N.; Le Guern, P.; Lagneau, V. Geometry and mineral heterogeneity controls on precipitation in fractures: An X-ray micro-tomography and reactive transport modeling study. *Adv. Water Resour.* **2021**, *152*, 103916.
(77) Masoudi, M.; Fazeli, H.; Miri, R.; Hellevang, H. Pore scale modeling and evaluation of clogging behavior of salt crystal aggregates in CO2-rich phase during carbon storage. *Int. J. Greenhouse Gas Control.* **2021**, *111*, 103475.
(78) Masoudi, M.; Nooraiepour, M.; Deng, H.; Hellevang, H. Mineral precipitation and geometry alteration in porous structures: How to upscale variations in permeability−porosity relationship? *Energy Fuels* **2024**, *38* (11), 9988−10001.
(79) Helgeson, H. C. Evaluation of irreversible reactions in geochemical processes involving minerals and aqueous solutions—I. Thermodynamic relations. *Geochim. Cosmochim. Acta* **1968**, *32* (8), 853−877.
(80) Helgeson, H. C.; Garrels, R. M.; MacKenzie, F. T. Evaluation of irreversible reactions in geochemical processes involving minerals and aqueous solutions—II. Applications. *Geochim. Cosmochim. Acta* **1969**, *33* (4), 455−481.
(81) Steefel, C. I.; Lasaga, A. C. A coupled model for transport of multiple chemical species and kinetic precipitation/dissolution reactions with application to reactive flow in single phase hydrothermal systems. *Am. J. Sci.* **1994**, *294* (5), 529−592.
(82) Steefel, C. I.*CRUNCHFLOW - Software For Modeling Multicomponent Reactive Flow And Transport. User's Manual*Lawrence Berkeley National Laboratory (LBNL)20091−91
(83) Li, Q.; Steefel, C. I.; Jun, Y.-S. Incorporating Nanoscale Effects into a Continuum-Scale Reactive Transport Model for CO2-Deteriorated Cement. *Environ. Sci. Technol.* **2017**, *51* (18), 10861−10871.
(84) Steefel, C. I.; Yang, L. Secondary magnesite formation from forsterite under CO2 sequestration conditions via coupled heterogeneous nucleation and crystal growth. *Geochim. Cosmochim. Acta* **2021**, *311*, 29−42.
(85) Hellevang, H.; Aagaard, P. Can the long-term potential for carbonatization and safe long-term CO2 storage in sedimentary formations be predicted? *Appl. GeoChem.* **2013**, *39*, 108−118.
(86) Aagaard, P.; Helgeson, H. C. Thermodynamic and kinetic constraints on reaction rates among minerals and aqueous solutions; I, Theoretical considerations. *Am. J. Sci.* **1982**, *282* (3), 237−285.
(87) Burton, W. K.; Cabrera, N.; Frank, F. C. The growth of crystals and the equilibrium structure of their surfaces. *Philos. Trans. R. Soc. Lond. A* **1951**, *243* (866), 299−358.
(88) Hellevang, H.; Pham, V. T.; Aagaard, P. Kinetic modelling of CO2−water−rock interactions. *Int. J. Greenhouse Gas Control.* **2013**, *15*, 3−15.
(89) Boampong, L. O.; Hyman, J. D.; Carey, W. J.; Viswanathan, H. S.; Navarre-Sitchler, A. Characterizing the combined impact of nucleation-driven precipitation and secondary passivation on carbon mineralization. *Chem. Geol.* **2024**, *663*, 122256.
(90) Prasianakis, N. I.; Curti, E.; Kosakowski, G.; Poonoosamy, J.; Churakov, S. V. Deciphering pore-level precipitation mechanisms. *Sci. Rep.* **2017**, *7*, 13765.

Downloaded from pubs.acs.org/cgdefu/article-pdf/26/18/7321/6451959/acs.cgd.6c00312.pdf by guest on 19 October 2026

https://doi.org/10.1021/acs.cgd.6c00312
Cryst. Growth Des. 2026, 26, 7321−7336

(91) Hellevang, H.; Wolff-Boenich, D.; Nooraiepour, M. Kinetic control on the distribution of secondary precipitates during CO_2-basalt interactions. *E3S Web Conf* **2019**, *98*, 04006.
(92) Nooraiepour, M.; Masoudi, M.; Shokri, N.; Hellevang, H. Probabilistic Nucleation and Crystal Growth in Porous Medium: New Insights from Calcium Carbonate Precipitation on Primary and Secondary Substrates. *ACS Omega* **2021**, *6* (42), 28072−28083.
(93) Gallo, Y. L.; Bildstein, O.; Brosse, E. Coupled reaction-flow modeling of diagenetic changes in reservoir permeability, porosity and mineral compositions. *J. Hydrol.* **1998**, *209* (1), 366−388.
(94) Beckingham, L. E. Evaluation of Macroscopic Porosity-Permeability Relationships in Heterogeneous Mineral Dissolution and Precipitation Scenarios. *Water Resour. Res.* **2017**, *53* (12), 10217−10230.
(95) Luhmann, A. J.; Tutolo, B. M.; Bagley, B. C.; Mildner, D. F. R.; Seyfried, W. E., Jr.; Saar, M. O. Permeability, porosity, and mineral surface area changes in basalt cores induced by reactive transport of CO2-rich brine. *Water Resour. Res.* **2017**, *53* (3), 1908−1927.
(96) Carman, P. C. *Flow of Gases through Porous Media*; Butterworths Scientific Publications: London, 1956.
(97) Verma, A.; Pruess, K. Thermohydrological conditions and silica redistribution near high-level nuclear wastes emplaced in saturated geological formations. *J. Geophys. Res. Solid Earth* **1988**, *93* (B2), 1159−1173.
(98) Thullner, M.; Zeyer, J.; Kinzelbach, W. Influence of Microbial Growth on Hydraulic Properties of Pore Networks. *Transp. Porous Media* **2002**, *49*, 99−122.
(99) Hommel, J.; Coltman, E.; Class, H. Porosity−Permeability Relations for Evolving Pore Space: A Review with a Focus on (Bio-)geochemically Altered Porous Media. *Transp. Porous Media* **2018**, *124*, 589−629.
(100) Deng, H.; Poonoosamy, J.; Molins, S. A reactive transport modeling perspective on the dynamics of interface-coupled dissolution-precipitation. *Appl. GeoChem* **2022**, *137*, 105207.
(101) Molins, S.; Soulaine, C.; Prasianakis, N. I.; Abbasi, A.; Poncet, P.; Ladd, A. J. C.; Starchenko, V.; Roman, S.; Trebotich, D.; Tchelepi, H. A.; Steefel, C. I. Simulation of mineral dissolution at the pore scale with evolving fluid-solid interfaces: Review of approaches and benchmark problem. *Comput. Geosci.* **2021**, *25*, 1285−1318.
(102) Yang, F.; Stack, A.; Starchenko, V. Micro-continuum approach for mineral precipitation. *Sci. Rep.* **2021**, *11*, 3495.
(103) Kile, D.; Eberl, D.; Hoch, A.; Reddy, M. An assessment of calcite crystal growth mechanisms based on crystal size distributions. *Geochim. Cosmochim. Acta* **2000**, *64* (17), 2937−2950.
(104) Vengrenovitch, R. On the ostwald ripening theory. *Acta Metall* **1982**, *30* (6), 1079−1086.
(105) Yang, F.; Yuan, K.; Stack, A. G.; Starchenko, V. Numerical Study of Mineral Nucleation and Growth on a Substrate. *ACS Earth Space Chem.* **2022**, *6* (7), 1655−1665.
(106) Wagner, T.; Kulik, D. A.; Hingerl, F. F.; Dmytrieva, S. V. Gem-selektor Geochemical Modeling Package: Tsolmod Library And Data Interface For Multicomponent Phase Models. *Can. Mineral.* **2012**, *50* (5), 1173−1195.
(107) Kulik, D. A.; Wagner, T.; Dmytrieva, S. V.; Kosakowski, G.; Hingerl, F. F.; Chudnenko, K. V.; Berner, U. R. GEM-Selektor geochemical modeling package: Revised algorithm and GEMS3K numerical kernel for coupled simulation codes. *Comput. Geosci.* **2013**, *17*, 1−24.
(108) Miron, G. D.; Kulik, D. A.; Dmytrieva, S. V.; Wagner, T. GEMSFITS: Code package for optimization of geochemical model parameters and inverse modeling. *Appl. GeoChem* **2015**, *55*, 28−45. Geochemical Speciation Codes and Databases
(109) Fischer, C.; Kurganskaya, I.; Schäfer, T.; Lüttge, A. Variability of crystal surface reactivity: What do we know? *Appl. GeoChem* **2014**, *43*, 132−157.
(110) Berger, O. Understanding the fundamentals of TiO2 surfaces. Part I. The influence of defect states on the correlation between crystallographic structure, electronic structure and physical properties of single-crystal surfaces. *Surf. Eng.* **2022**, *38*, 91−149.
(111) Liu, G.; Shih, A. J.; Deng, H.; Ojha, K.; Chen, X.; Luo, M.; McCrum, I. T.; Koper, M. T.; Greeley, J.; Zeng, Z. Site-specific reactivity of stepped Pt surfaces driven by stress release. *Nature* **2024**, *626*, 1005−1010.
(112) Clausen, C. M.; Batchelor, T. A. A.; Pedersen, J. K.; Rossmeisl, J. What Atomic Positions Determines Reactivity of a Surface? Long-Range, Directional Ligand Effects in Metallic Alloys. *Adv. Sci.* **2021**, *8* (9), 2003357.
(113) Schabernack, J.; Oliveira, A. F.; Heine, T.; Fischer, C. Variability of Radionuclide Sorption Efficiency on Muscovite Cleavage Planes. *Adv. Theory Simul.* **2023**, *6* (12), 2300406.
(114) Yuan, T.; Schymura, S.; Bollermann, T.; Molodtsov, K.; Chekhonin, P.; Schmidt, M.; Stumpf, T.; Fischer, C. Heterogeneous Sorption of Radionuclides Predicted by Crystal Surface Nanoroughness. *Environ. Sci. Technol.* **2021**, *55* (23), 15797−15809.
(115) Long, Z.; Liu, M.; Wu, X.-G.; Gu, K.; Yang, G.; Chen, Z.; Liu, Y.; Liu, R.; Zhong, H. A reactivity-controlled epitaxial growth strategy for synthesizing large nanocrystals. *Nat. Synth* **2023**, *2* (3), 296−304.
(116) Liu, L.; Sassi, M.; Zhang, X.; Nakouzi, E.; Kovarik, L.; Xue, S.; Jin, B.; Rosso, K. M.; De Yoreo, J. J. Understanding the mechanisms of anisotropic dissolution in metal oxides by applying radiolysis simulations to liquid-phase TEM. *Proc. Natl. Acad. Sci. U. S. A.* **2023**, *120* (23), No. e2101243120.
(117) Zhou, W.; Fischer, C. How Crystal Surface Reactivity Controls the Evolution of Surface Microtopography during Dissolution. *ACS Earth Space Chem.* **2025**, *9* (11), 2558−2566.
(118) Noiriel, C.; Oursin, M.; Daval, D. Examination of crystal dissolution in 3D: A way to reconcile dissolution rates in the laboratory? *Geochim. Cosmochim. Acta* **2020**, *273*, 1−25.
(119) Fischer, C.; Arvidson, R. S.; Lüttge, A. How predictable are dissolution rates of crystalline material? *Geochim. Cosmochim. Acta* **2012**, *98*, 177−185.
(120) Emmanuel, S.; Levenson, Y. Limestone weathering rates accelerated by micron-scale grain detachment. *Geology* **2014**, *42* (9), 751−754.
(121) Bibi, I.; Arvidson, R. S.; Fischer, C.; Lüttge, A. Temporal Evolution of Calcite Surface Dissolution Kinetics. *Minerals* **2018**, *8* (6), 256.
(122) Okonkwo, B. O.; Ming, H.; Zhang, Z.; Wang, J.; Rahimi, E.; Hosseinpour, S.; Davoodi, A. Microscale investigation of the correlation between microstructure and galvanic corrosion of low alloy steel A508 and its welded 309/308L stainless steel overlayer. *Corros. Sci.* **2019**, *154*, 49−60.
(123) Schabernack, J.; Fischer, C. Improved kinetics for mineral dissolution reactions in pore-scale reactive transport modeling. *Geochim. Cosmochim. Acta* **2022**, *334*, 99−118.
(124) Schabernack, J.; Fischer, C. Pulsating dissolution of crystalline matter: A surface-controlled process. *Geochim. Cosmochim. Acta* **2024**, *371*, 189−198.
(125) Arvidson, R. S.; Luttge, A. Mineral dissolution kinetics as a function of distance from equilibrium−New experimental results. *Chem. Geol.* **2010**, *269* (1), 79−88. Rates of Geochemical Processes and their Application to Natural Systems
(126) Dunn, T. H. *The effect of surface topography on crystallisation*; Ph.D. thesis, University of Leeds, 2023.
(127) Bots, P.; Benning, L. G.; Rodriguez-Blanco, J.-D.; Roncal-Herrero, T.; Shaw, S. Mechanistic insights into the crystallization of amorphous calcium carbonate (ACC). *Cryst. Growth Des.* **2012**, *12*, 3806−3814.
(128) Karthika, S.; Radhakrishnan, T.; Kalaichelvi, P. A review of classical and nonclassical nucleation theories. *Cryst. Growth Des.* **2016**, *16* (11), 6663−6681.
(129) Lutsko, J. F. How crystals form: A theory of nucleation pathways. *Sci. Adv.* **2019**, *5* (4), No. eaav7399.
(130) Verma, V.; Hodnett, B. K. A basis for the kinetic selection of polymorphs during solution crystallization of organic compounds. *CrystEngComm* **2018**, *20* (37), 5551−5561.
(131) Schneider, C.; Rasband, W.; Eliceiri, K. NIH Image to ImageJ: 25 years of image analysis. *Nat. Methods* **2012**, *9*, 671−675.

Downloaded from pubs.acs.org/cgdefu/article-pdf/26/18/7321/6451959/acs.cgd.6c00312.pdf by guest on 19 October 2026

https://doi.org/10.1021/acs.cgd.6c00312
Cryst. Growth Des. 2026, 26, 7321−7336

(132) Poonoosamy, J.; Obaied, A.; Deissmann, G.; Prasianakis, N. I.; Kindelmann, M.; Wollenhaupt, B.; Bosbach, D.; Curti, E. Microfluidic investigation of pore-size dependency of Barite nucleation. *Commun. Chem.* **2023**, *6* (1), 250. Cited by: 18; All Open Access, Gold Open Access, Green Open Access
(133) Santoso, R.; Guignon, L.; Deissmann, G.; Poonoosamy, J. Investigating the metastability of amorphous calcium carbonate by droplet microfluidics experiments using machine learning. *Sci. Rep.* **2025**, *15* (1), 05984.
(134) Poonoosamy, J.; Kaspor, A.; Schreinemachers, C.; Bosbach, D.; Cheong, O.; Kowalski, P. M.; Obaied, A. A radiochemical lab-on-a-chip paired with computer vision to unlock the crystallization kinetics of (Ba,Ra)SO4. *Sci. Rep.* **2024**, *14* (1), 9502. All Open Access, Gold Open Access, Green Open Access
(135) Martin, T. B.; Sutherland, D. R.; McDannald, A.; Kusne, A. G.; Beaucage, P. A. Autonomous Small-Angle Scattering for Accelerated Soft Material Formulation Optimization. *Chem. Mater.* **2025**, *37*, 4272−4281.
(136) Pyzer-Knapp, E. O.; Pitera, J. W.; Staar, P. W. J.; Takeda, S.; Laino, T.; Sanders, D. P.; Sexton, J.; Smith, J. R.; Curioni, A. Accelerating materials discovery using artificial intelligence, high performance computing and robotics, Cited by: 293; All Open Access, Gold Open Access, Green Open Access. *Npj Comput. Mater.* **2022**, *8* (1), 84.
(137) Boiger, R.; Xi, B.; Miron, G.-D.; Bonvin, M.; Provis, J. L.; Churakov, S. V.; Prasianakis, N. I. Machine learning-accelerated discovery of green cement recipes, Cited by: 3; All Open Access, Hybrid Gold Open Access. *Mater. Struct.* **2025**, *58* (5), 173.
(138) Nooraiepour, M.; Both, J. W.; Kadeethum, T.; Sadeghnejad, S. Partial Differential Equations in the Age of Machine Learning: A Critical Synthesis of Classical, Machine Learning, and Hybrid Methods. *arXiv* **2026**.
(139) Tsopanoglou, A.; Del Val, I. J. Moving towards an era of hybrid modelling: Advantages and challenges of coupling mechanistic and data-driven models for upstream pharmaceutical bioprocesses. *Curr. Opin. Chem. Eng.* **2021**, *32*, 100691.
(140) Glaser, J. I.; Benjamin, A. S.; Chowdhury, R. H.; Perich, M. G.; Miller, L. E.; Kording, K. P. Machine learning for neural decoding. *Eneuro* **2020**, *7* (4), 12.
(141) Jatnieks, J.; De Lucia, M.; Dransch, D.; Sips, M. Data-driven Surrogate Model Approach for Improving the Performance of Reactive Transport Simulations, Cited by: 39; All Open Access, Gold Open Access, Green Open Access. *Energy Procedia* **2016**, *97*, 447−453.
(142) Prasianakis, N. I.; Haller, R.; Mahrous, M.; Poonoosamy, J.; Pfingsten, W.; Churakov, S. V. Neural network based process coupling and parameter upscaling in reactive transport simulations. *Geochim. Cosmochim. Acta* **2020**, *291*, 126−143. Cited by: 51
(143) Prasianakis, N.; Laloy, E.; Jacques, D.; Meeussen, J.; Miron, G.; Kulik, D.; Idiart, A.; Demirer, E.; Coene, E.; Cochepin, B.; Leconte, M.; Savino, M.; Samper-Pilar, J.; De Lucia, M.; Churakov, S.; Kolditz, O.; Yang, C.; Samper, J.; Claret, F. Geochemistry and machine learning: Methods and benchmarking, Cited by: 7; All Open Access, Green Open Access, Hybrid Gold Open Access. *Environ. Earth Sci.* **2025**, *84* (5), 12066.
(144) Peng, H.; Rajyaguru, A.; Curti, E.; Grolimund, D.; Churakov, S. V.; Prasianakis, N. I. Towards digital twin of an in-situ experiment: A physics-enhanced machine-learning framework for inverse modelling of mass transport processes. *J. Hydrol.* **2026**, *664*, 134437. Cited by: 2; All Open Access, Hybrid Gold Open Access
(145) Raissi, M.; Perdikaris, P.; Karniadakis, G. Physics-informed neural networks: A deep learning framework for solving forward and inverse problems involving nonlinear partial differential equations, Cited by: 12697; All Open Access, Green Open Access. *J. Comput. Phys.* **2019**, *378*, 686−707.
(146) Lu, L.; Jin, P.; Pang, G.; Zhang, Z.; Karniadakis, G. E. Learning nonlinear operators via DeepONet based on the universal approximation theorem of operators, Cited by: 2158; All Open Access, Green Open Access. *Nat. Mach. Intell.* **2021**, *3*, 218−229.

Downloaded from pubs.acs.org/cgdefu/article-pdf/26/18/7321/6645195/acs.cgd.6c00312.pdf by guest on 19 October 2026

https://doi.org/10.1021/acs.cgd.6c00312
Cryst. Growth Des. 2026, 26, 7321−7336